Inhibition inputs from hippocampal CA1 to retrosplenial agranular cortex gate social behavior

Yuhan Shi[1], Jingjing Yan[1], Zhifang Chen[1], Xiaohong Xu[1], Zilong Qiu[1, 2, 3, *]

1 Institute of Neuroscience, State Key Laboratory of Neuroscience, Center for Excellence in Brain Science and Intelligence Technology, Chinese Academy of Sciences, Shanghai, China

2 Songjiang Hospital, Songjiang Institute, Shanghai Jiao Tong University School of Medicine

3 National Clinical Research Center for Aging and Medicine, Huashan Hospital, Fudan University, Shanghai, China

*Corresponding authors: Zilong Qiu, zqiu@ion.ac.cn

Lead contact: Zilong Qiu, zqiu@ion.ac.cn

ABSTRACT

Retrosplenial cortex has been implicated in processing sensory information and spatial learning. Abnormal neural activity in the retrosplenial cortex is found to be associated with psychedelics, as well as in mouse and non-human primate models of autism spectrum disorders (ASD). However, whether the retrosplenial cortex may directly regulate social behaviors remained unclear. In this work, we found that the neural activity of retrosplenial agranular cortex (RSA), a subregion of retrosplenial cortex, was initially activated, then quickly suppressed upon social contact. Interestingly, the up-down phase of RSA neurons is essential for normal social behaviors. We showed that PV-positive GABAergic neurons in the hippocampal CA1 region sent inhibitory projections to RSA. Blockade of the CA1-RSA inhibitory inputs significantly compromised social behavior. Remarkably, enhancing the

CA1-RSA inhibitory input was able to rescue defects of social behaviors in a mouse model for ASD. This work not only suggests a neural mechanism for salience processing of social behavior, but also provides a candidate brain region for ASD intervention with neural modulation approaches.

INTRODUCTION

Social behaviors are critical for survival and reproduction of mammals (Chen and Hong, 2018). Proceeding of social behaviors requires perception of sensory information, salience processing of social-related information and further integration in the prefrontal cortex (Kingsbury and Hong, 2020). Abnormal social behaviors associated with neuropsychiatric disorders, notably autism spectrum disorder(ASD), seriously affect the living condition of individuals (Bourgeron, 2015; Iakoucheva et al., 2019; Vorstman et al., 2017).

Recently, it was reported that ketamine treatment led to elevated neural activity in retrosplenial cortex (RSC) and scalable decreased social behaviors in mice (Vesuna et al., 2020). Moreover, we found that neural activity was abnormally upregulated in RSC of *MECP2* overexpressed mouse and functional connectivity of RSC associated with other brain regions were increased in the brain of non-human primate models for ASD, comparing to wild-type (WT) animals (Cai et al., 2020; Yu et al., 2020). Furthermore, our group, together with Li and colleagues, found that excitatory and inhibitory synaptic transmission in RSC are significantly altered in various genetic mouse models of ASD (Shang et al., 2021; Yang et al., 2021). Accumulated evidences suggest that RSC is implicated in regulating social behavior.

RSC is composed of two subregions, retrosplenial granular cortex (RSG) and retrosplenial agranular cortex (RSA), which are anatomically and functionally distinct with each other (Aggleton et al., 2021; Sigwald et al., 2019; Vogt, 2009). RSC receive synaptic inputs from numerous areas, including visual cortex, hippocampus, thalamic nuclei, as well as anteroventral nucleus (Brennan et al., 2021; Murakami et al., 2015;

Powell et al., 2020). In particular, the synaptic inputs to RSC from hippocampus are critical in memory formation and consolidation (Nitzan et al., 2020; Opalka and Wang, 2020; Yamawaki et al., 2019). Interestingly, we found that neural activity of hippocampal CA1 neurons were causally correlated to social behaviors in MECP2 overexpression mice, a mouse model for ASD (Sun et al., 2020).

During social behaviors, the salience processing of social vs. non-social inputs from sensory systems are fundamental for organisms to perform interactive behaviors with conspecific partners and further evoke social-related inter-brain neural activity in prefrontal cortex (Chen and Hong, 2018; Kingsbury and Hong, 2020). Thus, we hypothesized that the neural circuit from hippocampus to RSC plays a pivotal role in gating social behaviors via salience processing of sensory inputs, which are compromised by ASD-related genetic mutations.

In this work, we found that the neural activity of RSA neurons was initially activated, then quickly suppressed upon social contact. Interestingly, the up-down phase of RSA neurons is essential for social behaviors. Importantly, we identified that PV-positive interneurons in the hippocampal CA1 region send a long-range inhibitory projection to RSA. Blockade of the CA1-RSA inhibitory inputs significantly compromised social behavior. Remarkably, enhancing the CA1-RSA inhibitory input is able to rescue the defect of social interaction in an ASD mouse model. Together, these data demonstrated that the inhibition input from CA1 to RSA upon social contact functions as the salience control for proceeding of social behaviors, presumably via filtering out non-social sensory information in RSA regions. This work not only suggests a neural mechanism for salience processing of social information, but further provides a candidate brain region for ASD intervention with neural modulation approaches.

Results

Neural activity of RSA neurons exhibits an up-down phase during social interaction

First, we would like to investigate whether RSC neurons may be activated during the social interaction. We performed the immunostaining for c-fos, one of the immediately early gene for sensing neural activity, in the brain slice from mice after interacting with either stranger intruder mice or with objects for 1.5 hour in the home-cage experiment (Figure 1A-C). We found that the c-fos level in the RSA neurons of mice with stranger intruders were significantly increased comparing with mice with objects, suggesting that RSA neurons are activated upon social interaction (Figure 1D-F).

RSC has been implicated in integrating sensory information(Alexander and Nitz, 2015; Vann et al., 2009; Wolbers and Buchel, 2005). We aim to determine which subregion of RSC may receive input from sensory cortices. By injecting retrograde retroAAV-Cre-mCherry virus in to RSA or RSG regions of Ai-9 (Rosa26-CAG-loxp-stop-loxp-tdTomato) mice (Figure S1A-D), we found that RSA, but not RSG, primarily received inputs from the primary visual cortex (V1), suggesting that RSA may play an important role in relay information from sensory cortices to higher center during social interaction. We further performed anterograde tracing via injection of AAV-hSyn-ChR2-mCherry into V1 (Figures S1E). Abundant ChR2-mCherry-expressing axon terminals are found in RSA instead of RSG (Figures S1F), which is consistent with the previous finding in rat (Aggleton et al., 2021).

Although the expression c-fos could be quickly induced by neural activity, the protein level of c-fos will sustain for hours. In order to examine the dynamic of neural activity of RSA neurons during social interactive behavior, we injected AAV-CaMKII-GCaMP6s virus into RSA, followed by implantation of optic recording fiber. With this setup, we record the real-time of Ca^{2+} dynamics in RSA neurons with fiber photometry in layer IV-V of RSA in WT mice while mice performed social interaction in the home-cage task (Figure 1J). Surprisingly, we

found that the calcium transients were significantly declined right after sniffing stranger mice, comparing to mice sniffing novel objects (Figure 1K, L).

We next wonder whether RSA neuron may be inhibited by local GABAergic interneurons. To test this possibility, we injected AAV-DIO-GCaMP6s virus into VGAT-ires-Cre mice to specifically label GABAergic neurons in RSA (Figure 1M). Notably, we found that the calcium transients in GABAergic neurons of RSA also significantly declined a few seconds after social contact (Figure. 1N, O). Thus, we suggest that the activity of the excitatory and inhibitory neurons in RSA are quickly repressed by a strong inhibitory input during sniffing, although RSA neurons initially were activated with social contact.

Inhibition of RSA neurons after social contact facilitates social behavior

To further determine whether the up-down phase of RSA neurons is essential for social interactive behaviors, we set out to manipulate neural activity by optogenetics with the fine temporal resolution. To control activity of RSA neurons with the precise temporal resolution, we unilaterally injected AAV-harboring channelrhodopsin2 (ChR2) or Guillardia theta anion channel rhodopsin (GtACR) into RSA (Figure 2A). After 12 hours isolation, we examined whether the social interaction between the mouse in the home cage with a stranger mouse would be affected by manipulation of neural activity in RSA. We first continuously activated the excitatory neurons in RSA during social interaction by stimulating ChR2. Surprisingly, we found that with continuous activation of RSA neurons, mice exhibited significantly decrease social interaction, measured by cumulative sniffing time, interaction time, and interaction frequency, comparing to EYFP-expressing mice (Figure 2B-D).

Moreover, we examine whether continuous activation of RSA neurons may affect social behavior of mice in the classic three-chamber test. Consistently, we found that activation of RSA neurons led to completely loss of normal social preference with stranger vs. empty cages, as well as with stranger vs. with familiar partners (Figure 2E,

F). Furthermore, we found that the continuous activation of RSA did not change the anxiety level of mice in the open-field test, (Figure S2A, B). These data demonstrated that constantly activation of RSA strongly inhibits the social interaction behaviors of mice.

Next, we wonder whether inhibition of RSA neurons may affect social behaviors of mice. After injection of AAV-hSyn-GtACR into the RSA region, we could optogenetically inhibit the RSA neurons by photostimulation in various stages of social interaction (Figure 2A). First, we performed continuous inhibition by giving 550nm light to the RSA neurons. Interestingly, we found that the cumulative sniffing time and the sniffing frequency of mice with stranger intruder mice were also significantly declined, indicating that blockade of neural activity of RSA neurons may play negative roles in regulating social behaviors. Then we mimicked the down phase we discovered to inhibit neural activity right after sniffing starting (sniffing start-inhibition) (Figure 2A). Remarkably, we found that accumulative and single interaction time of mice with stranger mice after sniffing start-inhibition are significantly increased (Figure 2J-L), suggesting that suppression of neural activity of RSA neurons immediately after social contact enhance social interactive behaviors.

Therefore, we conclude that continuous activation or inhibition RSA neurons during social interaction will impair the social behaviors of mice, whereas the suppression of RSA neurons immediately after social contact is required for proper social interactive behaviors. The abnormalities in sensory information processing in ASD patients and animal models have been discovered (Wiggins et al., 2009). Correction of genetic defects in the sensory system could even rescue the behavioral defects in ASD mouse models. Thus, we hypothesize that this crucial suppression step in RSA may represent the filtering process for blocking non-social information within sensory inputs during social interaction.

PV-positive neurons in hippocampal CA1 project to RSA

We next set out to investigate where the inhibitory inputs to RSA neurons are from during social interaction. We first carried out the retrograde tracing by injecting cholera toxin B subunit (CTB) into RSA and found that there are numerous neurons were labeled in dorsal CA1 (Figure 3A). We next performed the immunostaining to characterize the subtype of labeled neurons. Surprisingly, we found that about 38% of the PV-positive neurons in CA1 were labeled by CTB (Figure 3A), suggesting that PV-positive neurons in CA1 may project to RSA. We also performed retrograde tracing by injecting retroAAV-hSyn-Cre-mCherry into RSA and AAV-DIO-GFP into CA1 (Figures S3A, B). We found that GFP and PV double positive neurons account for 23% of all the GFP positive neurons in CA1, further confirming the synaptic connection from PV-positive neurons from CA1 to RSA (Figures S3C-E).

We injected Cre-dependent AAV-DIO-ChR2-EYFP to label axon terminals, along with AAV-DIO-GFP to label soma, into CA1 of PV-Cre mice (Figure 3B). The ChR2-expressing axons were observed in layer II-III of the RSC neurons, indicating that PV-positive neurons sent extensive synaptic terminus to RSC (Figure 3B). We validated the observation by showing that almost all of GFP positive neuron were colocalized with PV signals.

To examine whether CA1 PV-positive neurons may form functional synaptic connections with RSA neurons, we applied an optogenetic-electrophysiological strategy to examine physiological synaptic currents in brain slice preparations. By injecting Cre-dependent AAV-DIO-ChR2-GFP virus in to CA1 of PV-Cre mice, we performed the whole-cell recording on layer IV-V neurons of RSA (Figure 3C). Upon the wide-filed photostimulation at 473 nm on ChR2-expressing axons, we found that RSA neurons exhibited outward inhibitory postsynaptic currents (IPSCs) at a command voltage of -10 mV, but no inward excitatory postsynaptic currents (EPSCs) by holding at −70 mV (Figure 3D, E). Furthermore, the IPSC can be fully blocked by the $GABA_A$ receptor antagonist SR55531, indicating that the IPSC was mediated by $GABA_A$ receptor (Figure 3E). Among 64 neurons recorded from 5 mice, the IPSCs

were recorded successfully in 16 neurons (Figure 3F). We then performed the whole-cell recording on the ChR2-EYFP expressing neurons in CA1 with photostimulation (Figure 3G). We found that recorded neurons show the fast-spiking pattern which is a key characteristic of the PV-positive GABAergic neurons, confirming the specificity of genetic labeling in mouse (Figure 3H).

Next, we would like to examine whether PV positive neurons in CA1 were responsive for social stimulus during social interactive behaviors. We performed immunostaining with c-fos in brain slices from mice interacting with either novel objects or stranger mice. We found that the c-fos level of PV-positive neurons in CA1 is significantly higher than in mice with stranger partners, comparing to with novel objects (Figure 3I, J). Thus, we found that a significant portion of PV-positive neurons in CA1 projected to RSA, which are activated by social stimulus and may in turn inhibit the RSA neurons during social behavior.

The inhibitory input from PV neurons in CA1 to RSA is crucial for social behavior

To investigate the role of the inhibitory input from PV-positive neurons in CA1to RSA for social behavior, we applied the pharmacogenetic approach by injecting AAV-DIO-mCherry or AAV-DIO-hM4D into CA1 of PV-Cre mice and implanting a pipette into the superficial layer of RSA to locally activate hM4D by infusing clozapine-N-oxide (CNO) (Figure 4A, B). In the same time, we injected AAV-CaMKII-GCaMP6s in RSA and implanted an optic recording fiber in layer IV-V of RSA to monito the real-time neural activity in RSA (Figure 4B).

During the home-cage test, we injected CNO into RSA through the implanted pipette and recorded calcium transients of RSA neuron during social interaction (Figure 4A, B). Consistently, we found that the decline phase of calcium transients during social interaction was completely blocked in the hM4D-expressing group, but not in the mCherry-expressing group (Figure 4C, D, F, G). Surprisingly, the social interaction of

mice was strongly impaired by blocking the inhibitory input from PV-positive neurons of CA1 to RSA in the hM4D-expressing group, comparing to the mCherry-expressing group (Figure 4E, H).

To further examine whether the CA1-PV-RSA inhibitory projection may affect social behaviors in the classic three-chamber test, we performed the social approach and social novelty tests for these mice (Figure 4I, J). After CNO treatment, we found that the preference in either the social approach test or the social novel test are strongly abolished in the hM4D-expressing group, comparing to the mCherry-expressing group, measured by the cumulative duration and frequency of social interaction (Figure 4K-N).

These data indicated that the inhibitory input from PV positive neurons of CA1 to RSA significantly contributed to the suppression of RSA neurons after social contact and was essential for proper social interactive behaviors.

Activation of the PV+ inhibitory projection from CA1 to RSA rescued the social deficit in a mouse model of ASD

Finally, we wonder whether enhancing the inhibitory projection from CA1 PV positive neurons to RSA may be able to rescue social deficits in ASD mouse models. Mutations of *MEF2C* were identified in individuals with ASD and intellectual disabilities (Gilissen et al., 2014). *Mef2c* haploinsufficient ($Mef2c^{+/-}$) mice exhibited ASD-like behaviors such as defects in the social interaction (Tu et al., 2017). Thus we asked whether enhancing the CA1 PV-RSA inhibitory pathway may be able to rescue social deficit phenotype of $Mef2c^{+/-}$ mice.

First, we validated previous finding by showing that $Mef2c^{+/-}$ mice indeed exhibited social deficit in the home-cage experiment (Figure S4A-C). Moreover, the population of PV-positive neurons decreased in CA1 of $Mef2c^{+/-}$ mice, as reported (Tu et al., 2017). To specifically target PV-positive neurons in the hippocampal CA1 region of

Mef2c$^{+/-}$ mice, we used a PV-specific enhancer to drive expression of either ChR2 (PV-ChR2) or mCherry (PV-mCherry) carried by AAV (Figure 5A) (Vormstein-Schneider et al., 2020). To confirm whether ChR2-labeled PV-positive neurons in CA1 of *Mef2c*$^{+/-}$ mice could project to RSA, we performed the whole-cell recording on RSA neurons with photostimulation at 473 nm (Figure 5A, B). We found that photo-activation ChR2-expression axons was able to evoke a robust IPSC in RSA neurons in brain slices post-synaptically, which could be totally blocked by SR55531, the antagonist of $GABA_A$ receptor (Figure 5B). Among 20 RSA neurons recorded, we found 6 neurons have positive responses (Figure S4F). Furthermore, by immunostaining PV-positive neurons in hippocampus, we found that over 80% of mCherry-positive neurons were co-labeled by PV, proving the specificity of the PV-specific enhancer (Figure 5C-F).

We then performed photostimulation in RSA continuously when mice performed the home-cage test. Consistently, we found that the overall interaction time and frequency was further decreased in the PV-ChR2 group of *Mef2c*$^{+/-}$ mice, comparing to the PV-mCherry group (Figure 5G-I). Notably, the social interactive time was significantly rescued in *Mef2c*$^{+/-}$ mice, if photostimulation for activating ChR2 was given right after sniffing starting (Figure 5J-L). These results demonstrate that activation of inhibitory projection of PV-positive neurons from CA1 to RSA during social contact was sufficient to rescue the impairment of social interaction in *Mef2c*$^{+/-}$ mice.

Discussion

Social behavior is one of fundamental behaviors in mammals, which may be called “interactive behaviors within community” in non-human mammalian species. Within community, the valence of social behavior is primarily influenced by social hierarchy and mating possibilities, whereas the salience of social behavior may largely be determined by how the brain process the social vs. non-social information. Salient processing of social-related information is a crucial step for proceeding of social

interaction behaviors. Moreover, the salience of social interaction is clearly compromised in people with ASD, a group of brain disorders with strong genetic predispositions.

The work by Vesuna et al. showed that abnormal elevated neural activity in RSC of mice caused by ketamine treatment led to dissociated behaviors including defects in social interaction in an interesting dose-dependent manner, which strongly implied that neural activity in RSC may play a critical role in salience processing for social interaction of animals(Vesuna et al., 2020). Together with our work and others, we showed that the synaptic transmission in RSC neurons were clearly disrupted in several ASD mice models including *Senp1*$^{+/-}$ and *Fmr1*$^{-/y}$ mice (Shang et al., 2021; Yang et al., 2021). In this work, we proposed a model in which the inhibitory projection from PV-positive neurons of CA1 to RSA serves as a salience processing node to filter out non-social information flowing through RSA from sensory cortices. Though how social information processing within RSA or RSC requires further work, the data presented here showed that there are neural mechanisms underlying the salience processing of social interaction behaviors. Since the hippocampus is one of brain regions extensively receiving sensory inputs besides sensory modules, we further postulated that the PV-positive neurons in the hippocampal CA1 region may serve as a salience processing switch by inhibiting the non-social sensory information in RSA upon social interaction, although all RSC neurons are firstly clearly activated by social interaction in the beginning.

Our finding further suggested that defects in salience processing in RSA may be the causative factor for abnormal social behaviors in ASD patients. Clinically, defects in sensory perception including visual and auditory systems are widely observed in people with ASD. However, whether the defect in sensory perception is one of causes or consequences of ASD remain debatable (Wiggins et al., 2009). This work suggests that defects in salience processing in RSA may be the causative factor for leading to

autistic-like behaviors, since enhancing this pathway would be able to rescue behavioral defects in mouse models for ASD.

RSC in human brain is easy to access with neural modulation approaches, such as transcranial magnetic stimulation. Thus our finding opened an important venue through which one may test this hypothesis by manipulating neural activity in RSC in people with ASD and explore potential intervene methods.

Availability of data and materials

The datasets used and/or analyzed in the current study are available from the lead contact on the reasonable request.

Competing interests

The authors declare that they have no competing interests.

Acknowledgements

We thank Dr. Xiaowei Chen, Yu Fu and members of NPC for providing valuable comments for the manuscript. This work was supported by grants from the NSFC Grants (#81941015, #82021001); Strategic Priority Research Program of the Chinese Academy of Sciences (XDB32060202); Program of Shanghai Academic Research Leader, and the Science and Technology Commission of Shanghai Municipality (#2018SHZDZX05), Z.Q. is supported by GuangCi Professorship Program of Ruijin Hospital Shanghai Jiao Tong University School of Medicine.

References

Aggleton, J.P., Yanakieva, S., Sengpiel, F., and Nelson, A.J. (2021). The separate and combined properties of the granular (area 29) and dysgranular (area 30) retrosplenial

cortex. Neurobiology of learning and memory *185*, 107516.

Alexander, A.S., and Nitz, D.A. (2015). Retrosplenial cortex maps the conjunction of internal and external spaces. Nature neuroscience *18*, 1143-1151.

Bourgeron, T. (2015). From the genetic architecture to synaptic plasticity in autism spectrum disorder. Nature reviews Neuroscience *16*, 551-563.

Brennan, E.K., Jedrasiak-Cape, I., Kailasa, S., Rice, S.P., Sudhakar, S.K., and Ahmed, O.J. (2021). Thalamus and claustrum control parallel layer 1 circuits in retrosplenial cortex. eLife *10*.

Cai, D.C., Wang, Z., Bo, T., Yan, S., Liu, Y., Liu, Z., Zeljic, K., Chen, X., Zhan, Y., Xu, X., *et al.* (2020). MECP2 Duplication Causes Aberrant GABA Pathways, Circuits and Behaviors in Transgenic Monkeys: Neural Mappings to Patients with Autism. The Journal of neuroscience : the official journal of the Society for Neuroscience *40*, 3799-3814.

Chen, P., and Hong, W. (2018). Neural Circuit Mechanisms of Social Behavior. Neuron *98*, 16-30.

Gilissen, C., Hehir-Kwa, J.Y., Thung, D.T., van de Vorst, M., van Bon, B.W., Willemsen, M.H., Kwint, M., Janssen, I.M., Hoischen, A., Schenck, A., *et al.* (2014). Genome sequencing identifies major causes of severe intellectual disability. Nature *511*, 344-347.

Iakoucheva, L.M., Muotri, A.R., and Sebat, J. (2019). Getting to the Cores of Autism. Cell *178*, 1287-1298.

Kingsbury, L., and Hong, W. (2020). A Multi-Brain Framework for Social Interaction. Trends in neurosciences *43*, 651-666.

Murakami, T., Yoshida, T., Matsui, T., and Ohki, K. (2015). Wide-field Ca(2+) imaging reveals visually evoked activity in the retrosplenial area. Frontiers in molecular neuroscience *8*, 20.

Nitzan, N., McKenzie, S., Beed, P., English, D.F., Oldani, S., Tukker, J.J., Buzsaki, G., and Schmitz, D. (2020). Propagation of hippocampal ripples to the neocortex by way of a subiculum-retrosplenial pathway. Nature communications *11*, 1947.

Opalka, A.N., and Wang, D.V. (2020). Hippocampal efferents to retrosplenial cortex and lateral septum are required for memory acquisition. Learning & memory *27*, 310-318.

Powell, A., Connelly, W.M., Vasalauskaite, A., Nelson, A.J.D., Vann, S.D., Aggleton, J.P., Sengpiel, F., and Ranson, A. (2020). Stable Encoding of Visual Cues in the Mouse Retrosplenial Cortex. Cerebral cortex *30*, 4424-4437.

Shang, H.-F., Cai, R., Sun, H., Sheng, T., Lian, Y.-N., Liu, L., Chen, W., Gao, L., Xu, H., Zhang, C., *et al.* (2021). Deconstruction of the retrosplenial granular cortex for social behavior in the mouse model of fragile X syndrome. bioRxiv.

Sigwald, E.L., Bignante, E.A., de Olmos, S., and Lorenzo, A. (2019). Fear-context

association during memory retrieval requires input from granular to dysgranular retrosplenial cortex. Neurobiology of learning and memory *163*, 107036.

Sun, L., Chen, R., Li, L., Yuan, B., Song, K., Pan, N., Cheng, T.-L., Chang, S., Lin, K., He, X., *et al.* (2020). Visualization and correction of social abnormalities-associated neural ensembles in adult MECP2 duplication mice. Science Bulletin *65*, 1192-1202.

Tu, S., Akhtar, M.W., Escorihuela, R.M., Amador-Arjona, A., Swarup, V., Parker, J., Zaremba, J.D., Holland, T., Bansal, N., Holohan, D.R., *et al.* (2017). NitroSynapsin therapy for a mouse MEF2C haploinsufficiency model of human autism. Nature communications *8*, 1488.

Vann, S.D., Aggleton, J.P., and Maguire, E.A. (2009). What does the retrosplenial cortex do? Nature reviews Neuroscience *10*, 792-802.

Vesuna, S., Kauvar, I.V., Richman, E., Gore, F., Oskotsky, T., Sava-Segal, C., Luo, L., Malenka, R.C., Henderson, J.M., Nuyujukian, P., *et al.* (2020). Deep posteromedial cortical rhythm in dissociation. Nature *586*, 87-94.

Vogt, B.A. (2009). CHAPTER 1 Regions and Subregions of the Cingulate Cortex.

Vormstein-Schneider, D., Lin, J.D., Pelkey, K.A., Chittajallu, R., Guo, B., Arias-Garcia, M.A., Allaway, K., Sakopoulos, S., Schneider, G., Stevenson, O., *et al.* (2020). Viral manipulation of functionally distinct interneurons in mice, non-human primates and humans. Nature neuroscience *23*, 1629-1636.

Vorstman, J.A.S., Parr, J.R., Moreno-De-Luca, D., Anney, R.J.L., Nurnberger, J.I., Jr., and Hallmayer, J.F. (2017). Autism genetics: opportunities and challenges for clinical translation. Nature reviews Genetics *18*, 362-376.

Wiggins, L.D., Robins, D.L., Bakeman, R., and Adamson, L.B. (2009). Brief report: sensory abnormalities as distinguishing symptoms of autism spectrum disorders in young children. Journal of autism and developmental disorders *39*, 1087-1091.

Wolbers, T., and Buchel, C. (2005). Dissociable retrosplenial and hippocampal contributions to successful formation of survey representations. The Journal of neuroscience : the official journal of the Society for Neuroscience *25*, 3333-3340.

Yamawaki, N., Corcoran, K.A., Guedea, A.L., Shepherd, G.M.G., and Radulovic, J. (2019). Differential Contributions of Glutamatergic Hippocampal-->Retrosplenial Cortical Projections to the Formation and Persistence of Context Memories. Cerebral cortex *29*, 2728-2736.

Yang, K., Shi, Y., Du, X., Zhang, Y., Shan, S., Yuan, Y., Wang, R., Zhou, C., Liu, Y., Cai, Z., *et al.* (2021). SENP1 in the retrosplenial agranular cortex regulates core autistic-like symptoms in mice. bioRxiv preprint.

Yu, B., Yuan, B., Dai, J.K., Cheng, T.L., Xia, S.N., He, L.J., Yuan, Y.T., Zhang, Y.F., Xu, H.T., Xu, F.Q., *et al.* (2020). Reversal of Social Recognition Deficit in Adult Mice with MECP2 Duplication via Normalization of MeCP2 in the Medial Prefrontal Cortex. Neuroscience bulletin *36*, 570-584.

Figure legends

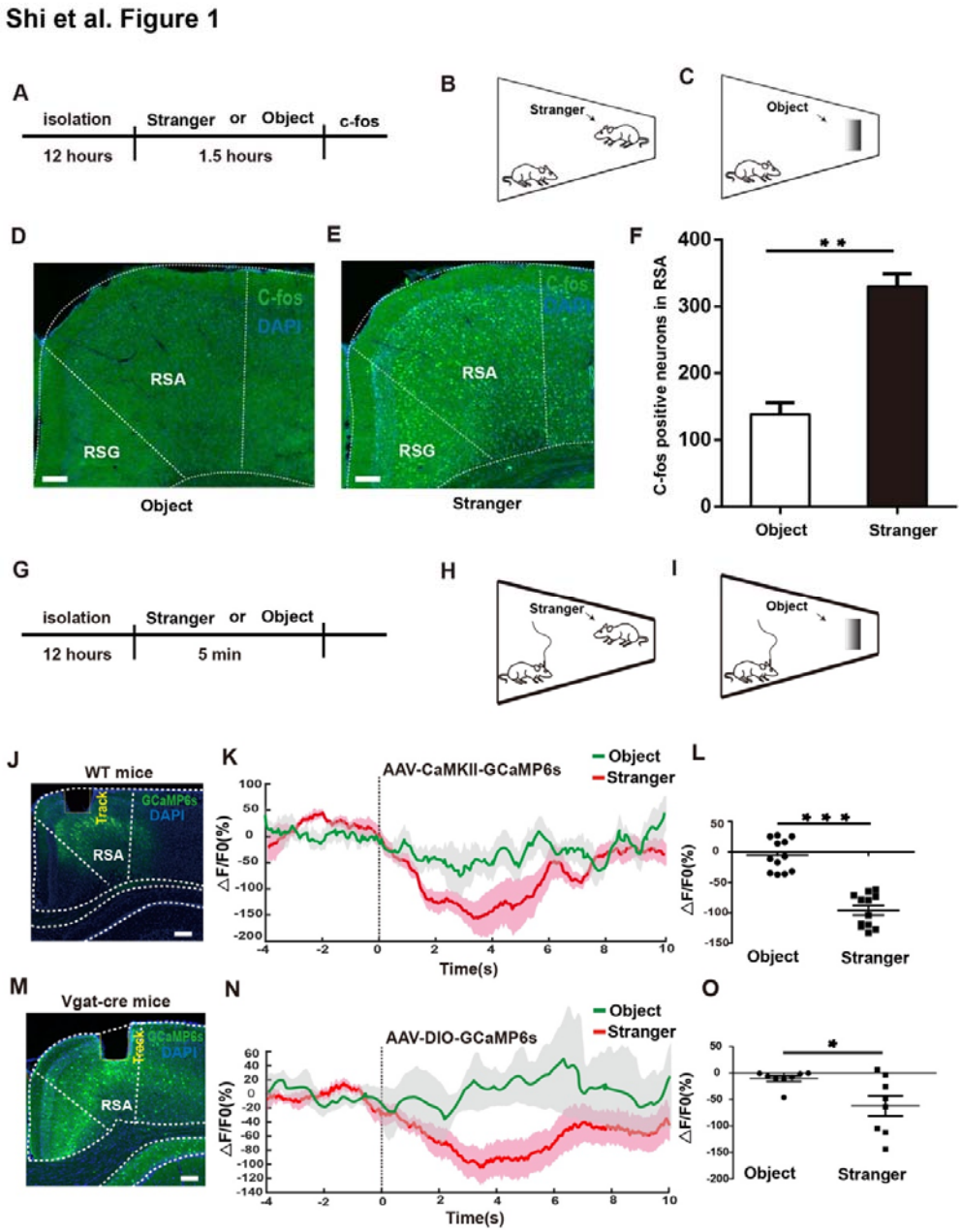

Figure 1. RSA is activated by social contact and inhibited after sniffing initiation

(A-C) Schematic illustration of the home-cage test.

Representative images showing c-fos expression in RSA after interaction with object (D) and stranger mice (E). Scale bar, 300μm.

(F) Quantification of numbers of c-fos positive neurons in RSA from (D, E).

(G-H) Schematic illustration of the home-cage test for fiber-photometry experiment.

(J) Implantation of the optic fiber for fiber photometry in RSA layer IV-V of a WT mouse injected with AAV-CaMKII-GCaMP6s. Scale bar, 250μm.

(K) Mean calcium transient associated with social interaction. Solid lines indicate mean and shadow areas indicate SEM (green: object, red: stranger). Dash line at the 0s time point represents the time point when mice actively touched the stranger mice with nose.

(L) Quantification of average ΔF/F value of (0-6s) from mice with either objects or stranger mice (baseline is the mean value of -4s-0s) (n = 12 mice for each group).

(M) Implantation of the optic fiber for fiber photometry in RSA of the Vgat-cre mouse injected with AAV-DIO-GCaMP6s. Scale bar, 250μm.

(N) Mean calcium transient associated with social interaction process. Solid lines indicate mean and shadow areas indicate SEM (green: object, red: stranger). Dash line at the 0s time point represents the time point when the mice actively touched the stranger mice with nose.

(O) Quantification of average ΔF/F value of (0-6s) from mice with either objects or stranger mice (baseline is the mean value of -4s-0s) (n = 8 mice for each group).

*$p < 0.05$, ** $p < 0.01$, *** $p < 0.001$. Error bars represent mean ± SEM.

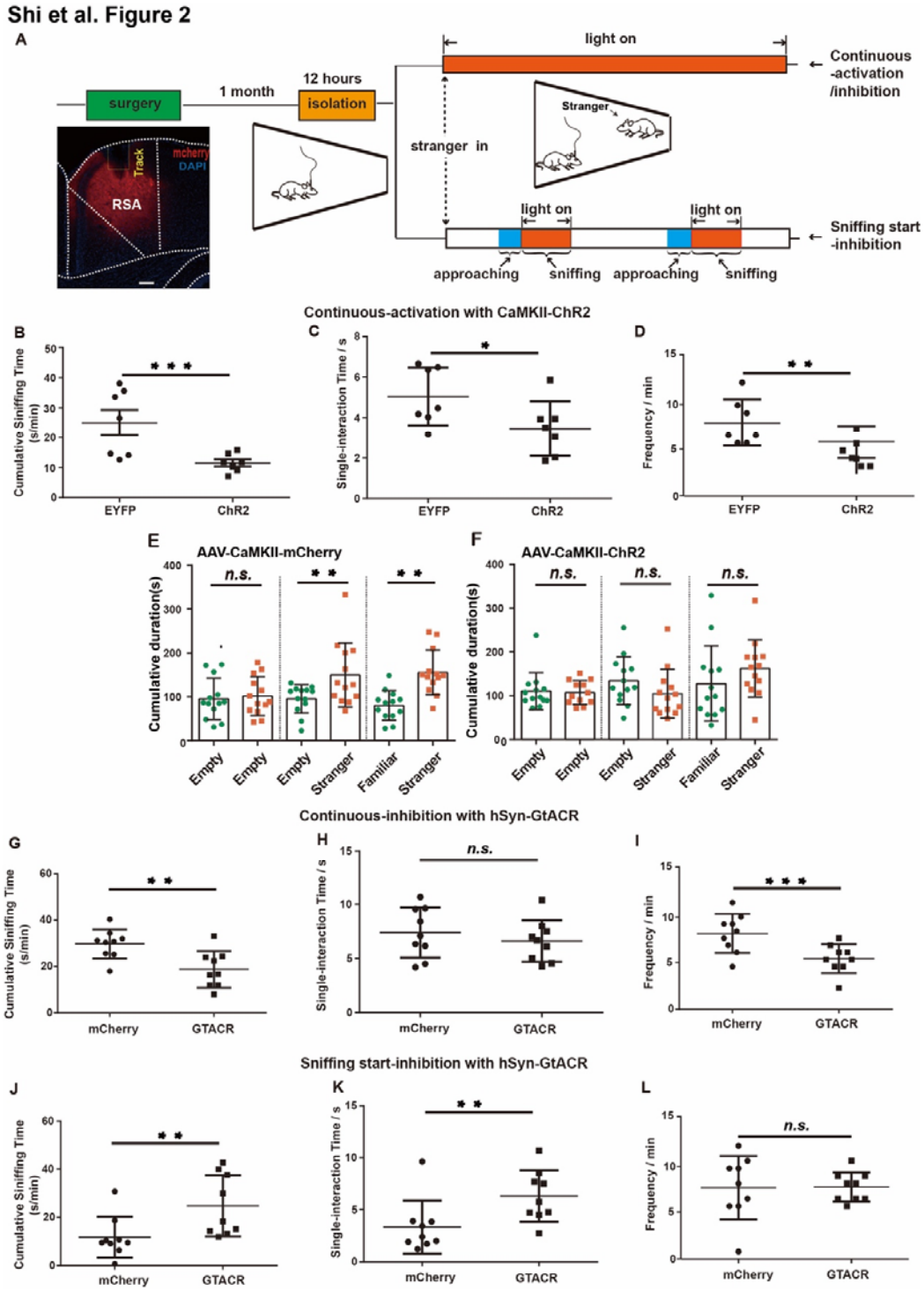

Figure 2. Sniffing-start inhibition of RSA facilitates the home-cage social behavior

(A) Schematic illustration of the optogenetic manipulation in RSA of mice injected with either AAV-ChR2-mCherry or AAV-GtACR during social interaction in home-cage tests. Scale bar, 600μm.

Quantification of cumulative sniffing time (B), single-interaction time (C) and sniffing frequency (C) induced by continuous 473 nm light activation in the ChR2 group and the EYFP group.

Quantification of cumulative duration during social approach and social novelty sessions in the three-chamber test for the mCherry group (E) or the ChR2 group (F) (n = 13 mice for each group).

Quantification of cumulative sniffing time (G), single-interaction time (H) and sniffing frequency (I) induced by continuous 550nm light inhibition in the GtACR group, comparing to the mCherry group (n = 9 mice for each group).

Quantification of cumulative sniffing time (J), single-interaction time (K) and sniffing frequency (L) induced by sniffing-start 550nm light inhibition in the GtACR group, comparing to the mCherry group (n = 9 mice for each group).

*$p < 0.05$, ** $p < 0.01$, *** $p < 0.001$. Error bars represent mean ± SEM.

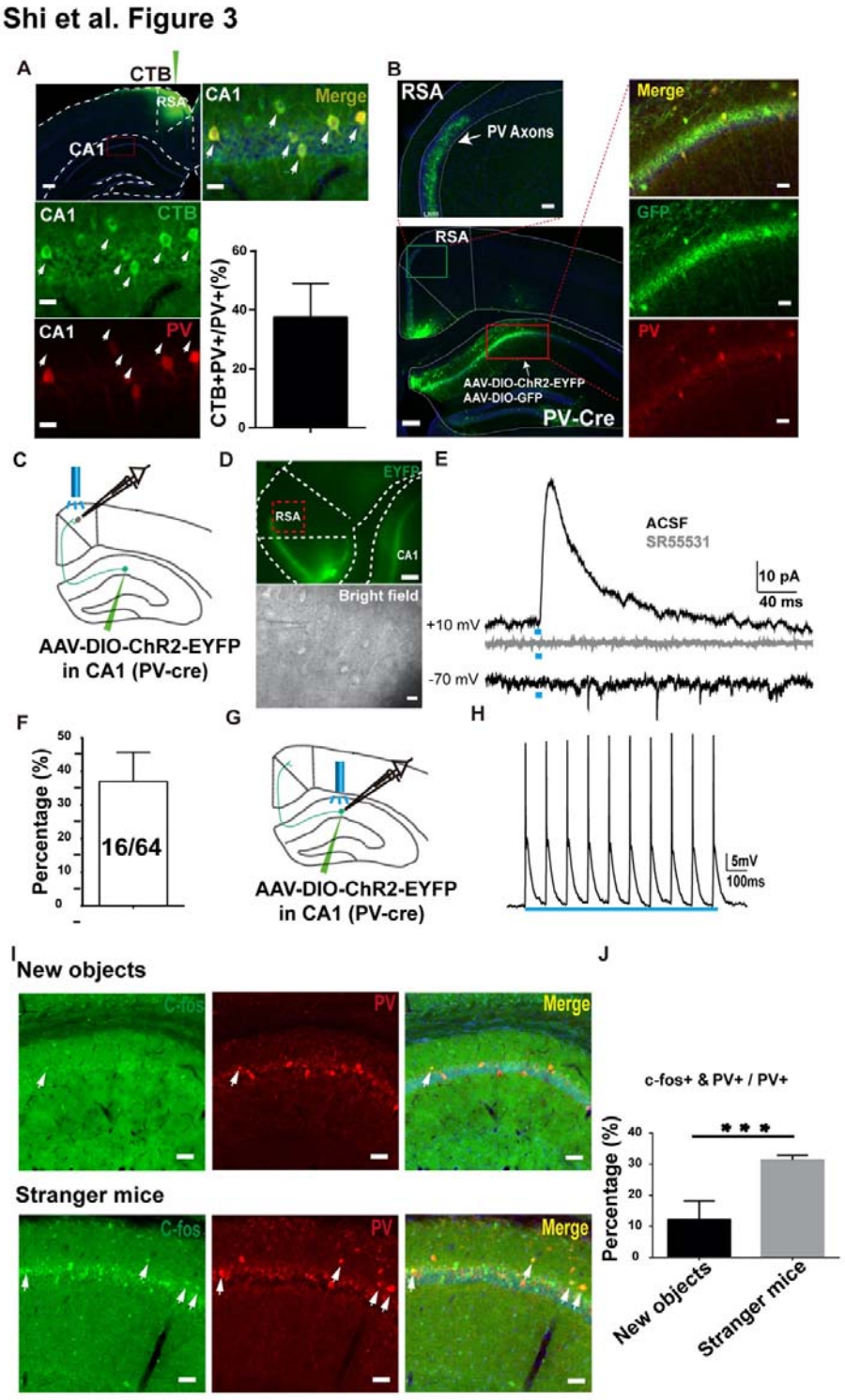

Figure 3. CA1 PV-positive neurons project to RSA and activated by social behavior.

(A) Representative images showing retrograde tracing of RSA neurons with CTB. Quantification of the percentage of CTB and PV double positive neurons in total PV-positive neurons in CA1 (lower right panel). Scale bar, 750μm (upper left panel), 10μm (three zoomed-in areas of CA1).

(B) Illustration of the axon terminal of the CA1 PV+ neurons in RSA (upper left panel), scale bar, 80μm; and the CA1 injection site of the of the virus; scale bar, 600μm (lower left panel), 20μm (three zoomed-in regions of CA1).

(C) Schematic illustration of the patch-clamp recording on RSA neurons and simultaneously activating the CA1 PV axon terminal using 473 nm light.

(D) Representative images of the patch-clamp recording under the infrared microscope illuminated by epifluorescence (upper panel), scale bar, 400μm and infrared-differential interference contrast illumination (bright field), scale bar, 10μm.

(E) The representative trace (upper) of the recorded IPSCs on RSA neurons activated by 473 nm light with a +10mV holding potential which was abolished by $GABA_A$ receptor antagonist SR55531(gray trace). The representative trace recorded on RSA neurons activated by 473 nm light with a -70mV holding potential (lower).

(F) The evoked IPSCs were identified on 16 neurons of 64 neurons recorded from 5 mice.

(G) Schematic illustration of the patch-clamp recording on CA1 PV-positive neurons with activating the recorded neurons using 473 nm light in PV-cre mice injected with AAV-DIO-ChR2-EYFP into CA1.

(H) The spikes recorded on EYFP-labeled neurons in CA1 of PV-cre mice with activated by stimulation of 473 nm light.

(I) Representative images of c-fos expression in CA1 PV+ neurons of mice with objects (upper three panels) and stranger mice (lower three panels) in the home-cage test. Scale bar, 20μm.

(J) Quantification of percentage of PV and c-fos double positive neurons in total PV-positive neurons in mice with new objects or with stranger mice (n= 18 slices from 3 mice of each group).

***$p < 0.001$. Error bars represent mean ± SEM.

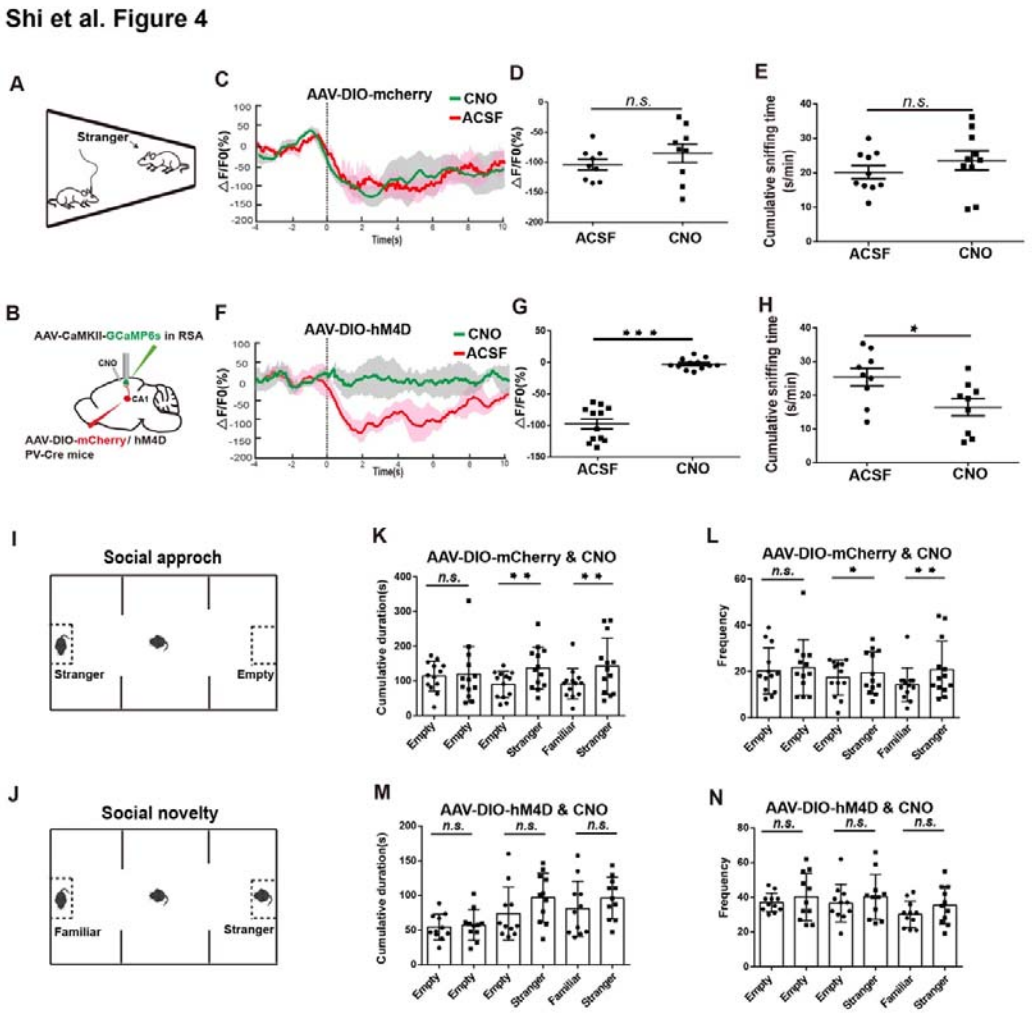

Figure 4 Blockade of the inhibitory projection from PV-positive neurons in CA1 to RSA abolished the inactivation in RSA during social behavior and led to social deficit.

(A, B) Schematic illustration of set-up for the home-cage test and the pharmacogenetic manipulation with fiber-photometry recording on RSA excitatory neurons. AAV-DIO-mCherry/hM4D were injected into CA1 of PV-Cre mice and AAV-CaMKII-CCaMP6s were injected to RSA, with implantation of the optic recording fiber and pipette for CNO infusion.

(C) Calcium transient of mice injected with AAV-DIO-mCherry during social interaction process (n= 9 mice for each group). Solid lines indicate mean values and shadow areas indicate SEM (green: CNO, red: ACSF). Dash line in the 0s time point

represents the time point when the experimental mice actively touched the stranger mice with nose.

(D) Quantification of average ΔF/F value of 0-6s (baseline is the mean value of -4s-0s) from mice in either the ACSF group and the CNO group (n = 9 mice for each group).

(E) Quantification of the cumulative sniffing time in the ACSF group and the CNO group in home-cage test (n = 10 mice for each group).

(F) Calcium transient of mice injected with AAV-DIO-hM4D during social interaction process (n= 12 mice for each group). Solid lines indicate mean value and shadow areas indicate SEM (green: CNO, red: ACSF).

(G) Quantification of average ΔF/F value of 0-6s (baseline is the mean value of -4s-0s) from the ACSF group and the CNO group (n = 9 mice for each group).

(H) Quantification of the cumulative sniffing time in the ACSF group and the CNO group in home-cage tests (n = 9 mice for each group).

(I, J) Schematic illustration of social approach (I) and social novelty (J) session of the three-chamber test.

Quantification of social time (K) and frequency (L) in the three-chamber test for in the mCherry group injected with CNO (n = 13 mice for each group).

Quantification of social time (M) and frequency (N) in the three-chamber test for the hM4D group injected with CNO (n = 11 mice for each group).

* $p < 0.05$, ** $p < 0.01$, *** $p < 0.001$. Bars represent mean ± SEM.

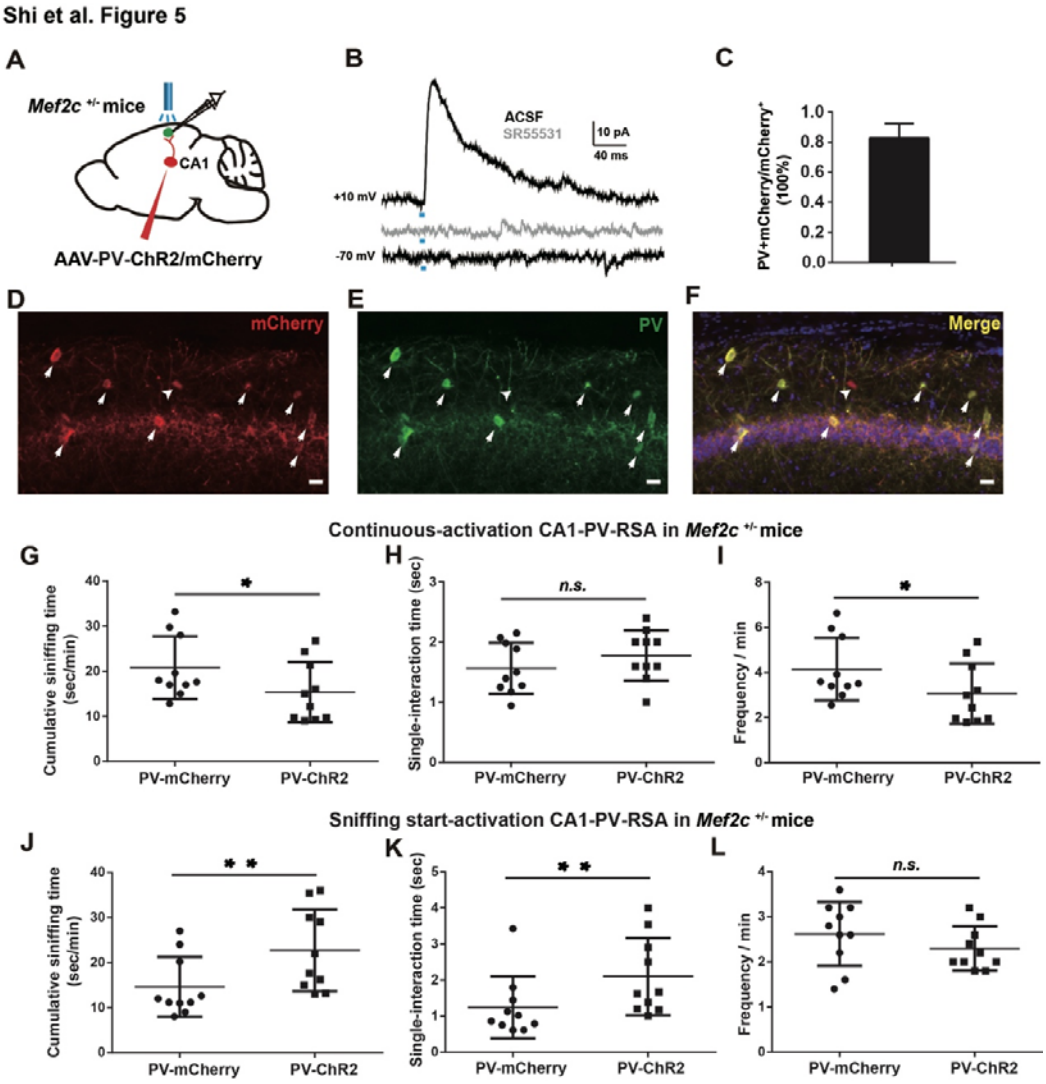

Figure 5 Activating the inhibitory projection from CA1 PV-positive neurons to RSA after sniffing initiation rescued the social deficit in *Mef2c*$^{+/-}$ mice

(A) Schematic illustration for optogenetic manipulation of PV-positive input to RSA in *Mef2c*$^{+/-}$ mice. AAV-PV-ChR2-mCherry was injected at CA1 of *Mef2c*$^{+/-}$ mice with implantation of optic stimulation fiber in RSA.

(B) The representative trace (upper) of the recorded IPSCs on RSA neurons activated by 473 nm light with a +10mV holding potential which was abolished by $GABA_A$ receptor antagonist SR55531(gray trace), and the representative trace recorded on RSA neurons activated by 473 nm light with a -70mV holding potential (lower).

Immunostaining of PV and mCherry in hippocampal slices of *Mef2c*$^{+/-}$ mice injected with AAV-PV-ChR2-mCherry (C-F).

(C) Quantification of the percentage of mCherry and PV double positive neurons account for mCherry positive neurons in CA1. Scale bar, 10μm.

Quantification of cumulative sniffing time (G), single-interaction time (H) and sniffing frequency (I) induced by continuous 473 nm light activation in the PV-ChR2 group and the PV-mCherry group.

Quantification of cumulative sniffing time (J), single-interaction time (K) and sniffing frequency (L) induced by sniffing-start 473 nm light activation in the PV-ChR2 group and the PV-mCherry group.

* $p < 0.05$, ** $p < 0.01$. Error bars represent mean ± SEM.

Shi et al. Figure 1

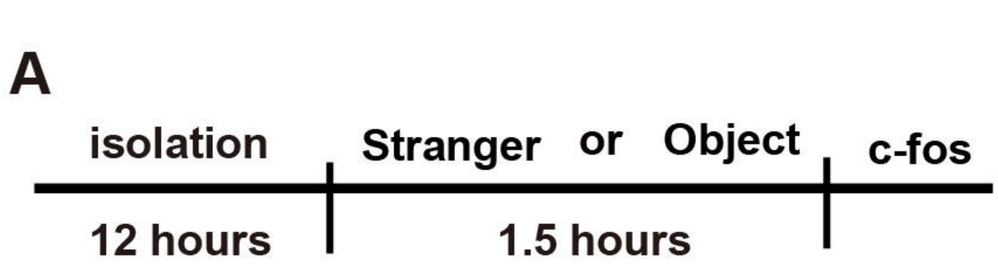

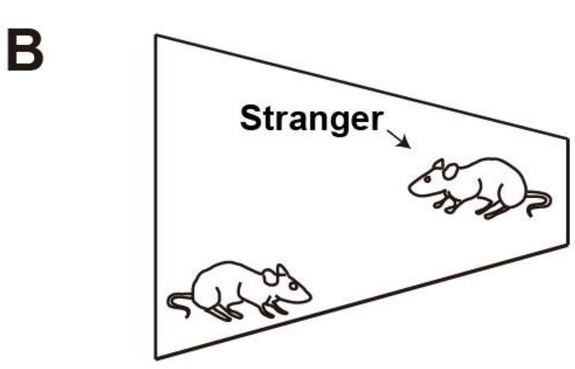

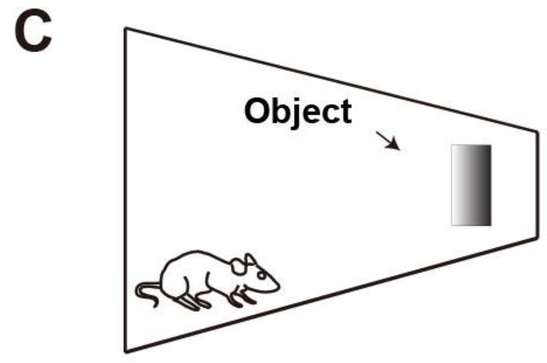

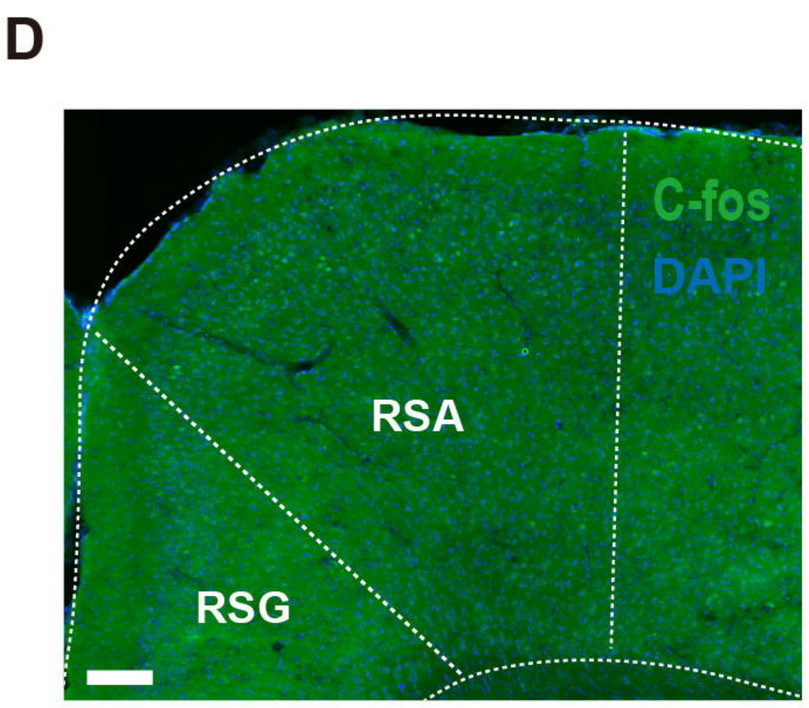

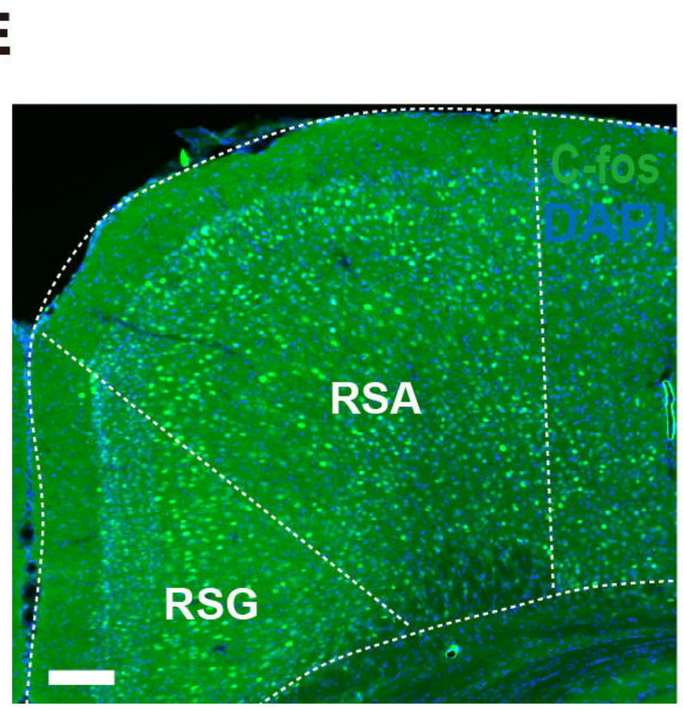

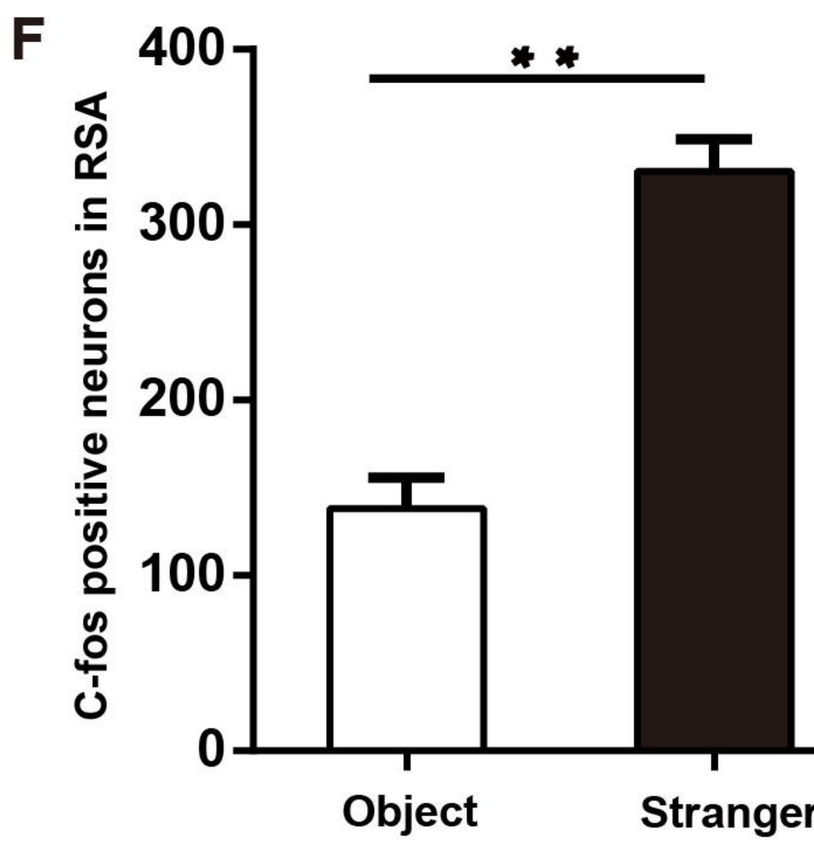

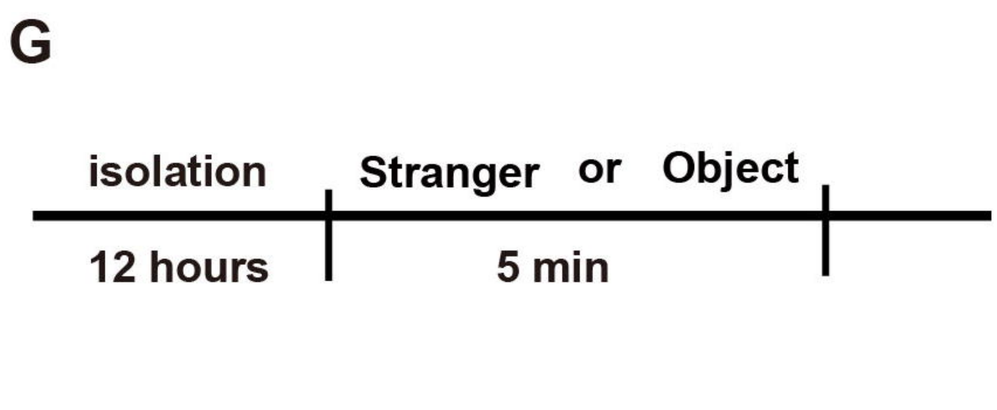

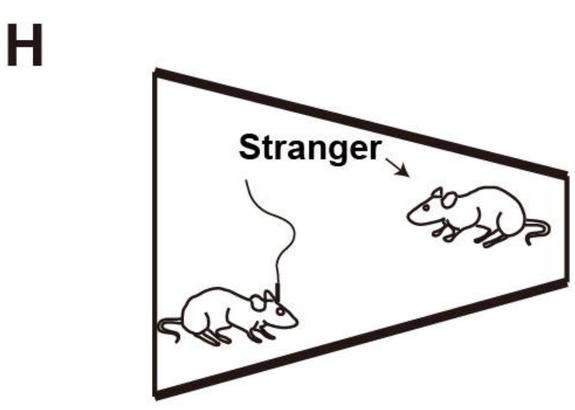

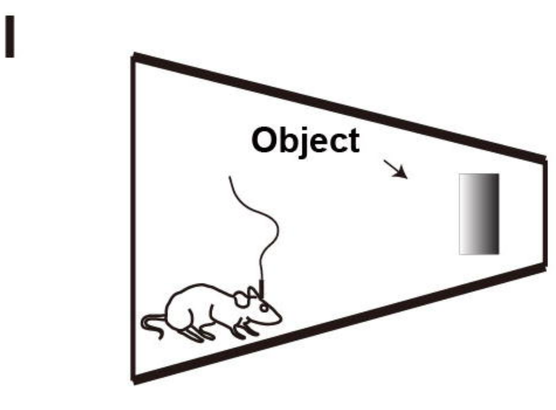

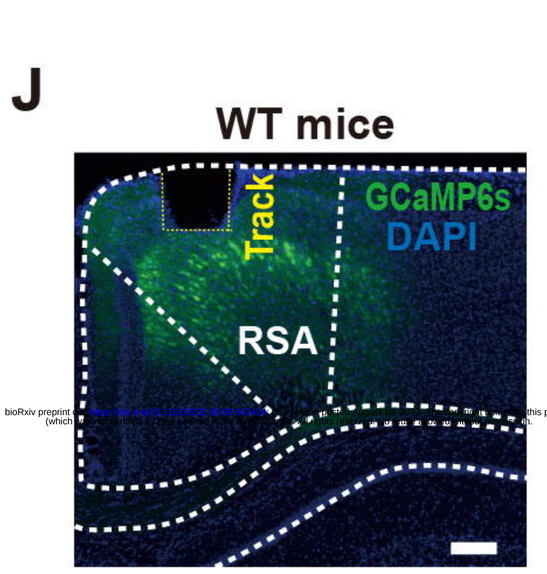

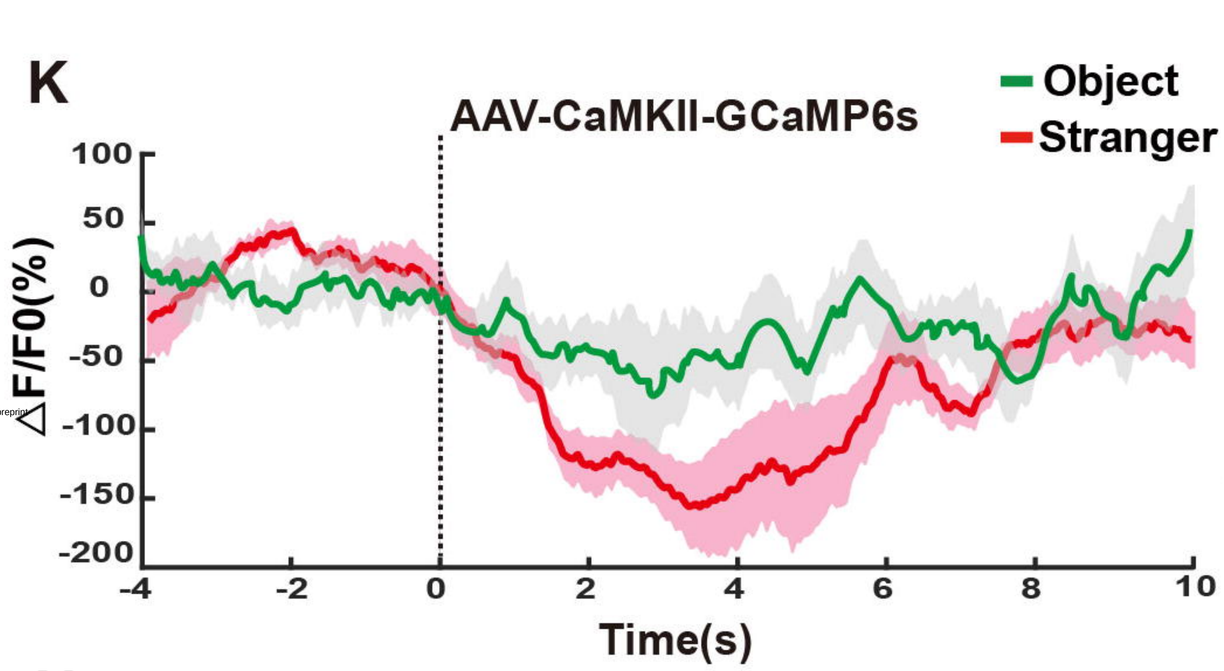

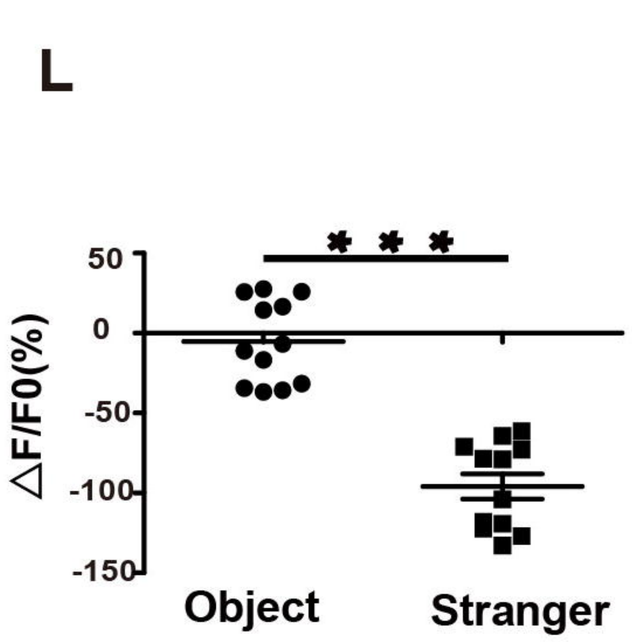

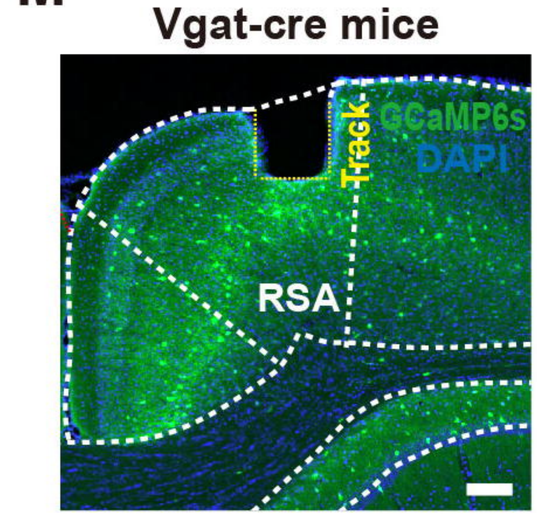

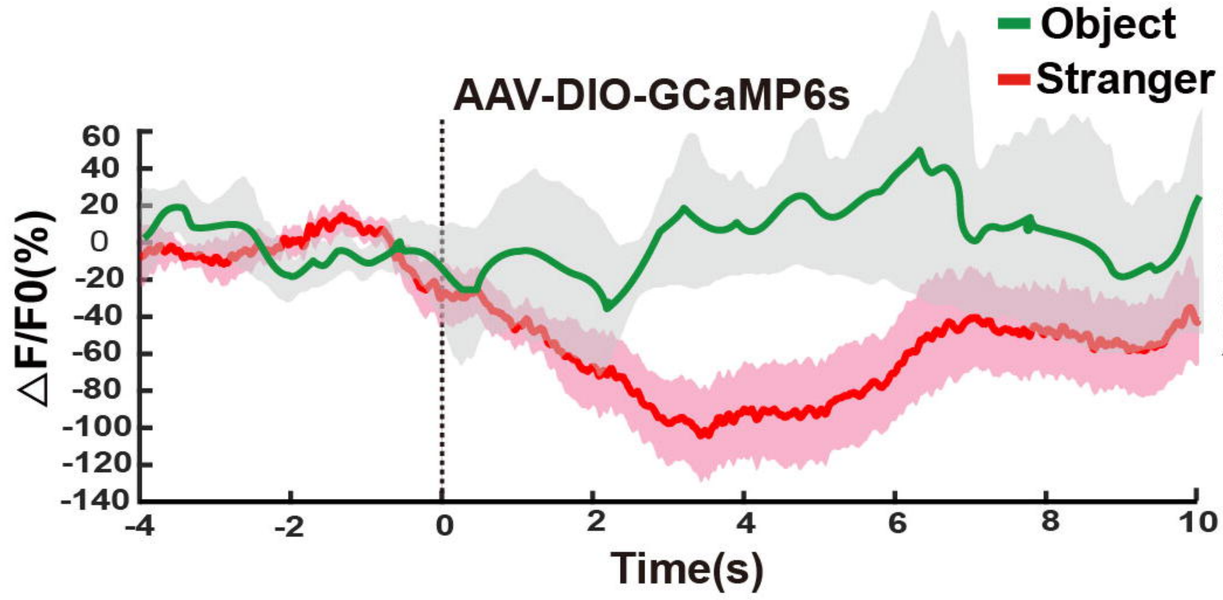

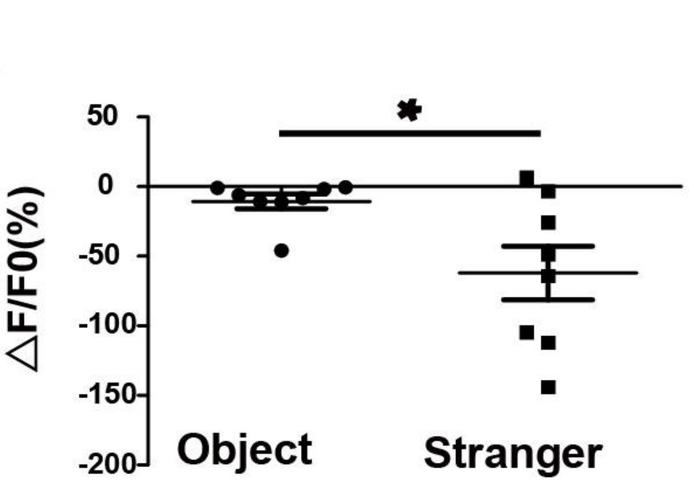

Shi et al. Figure 2

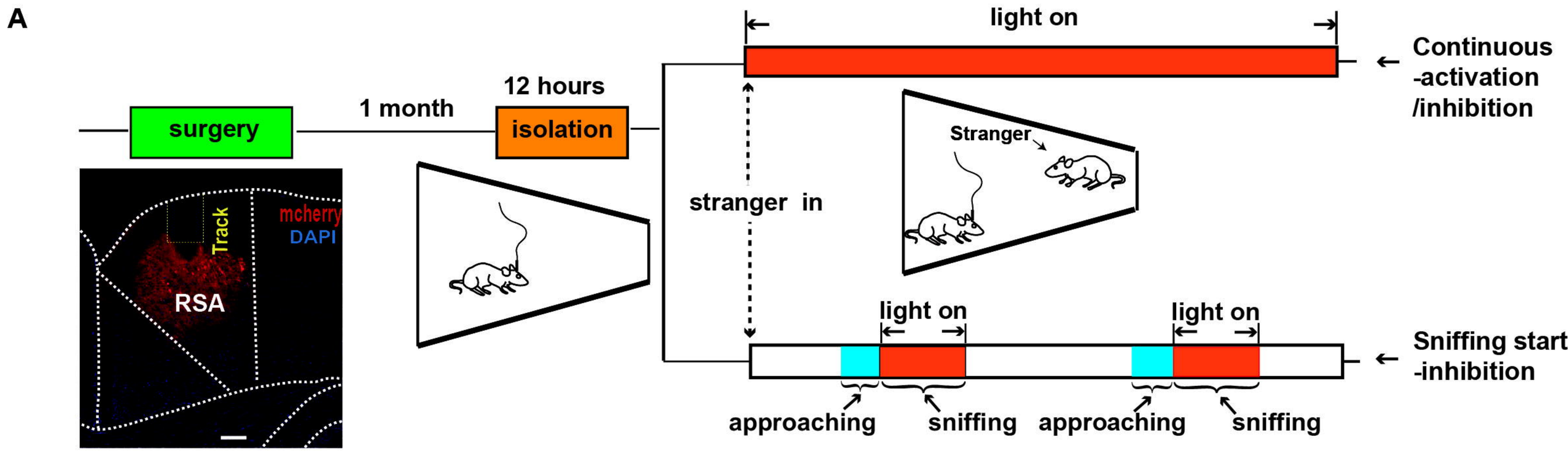

Continuous-activation with CaMKII-ChR2

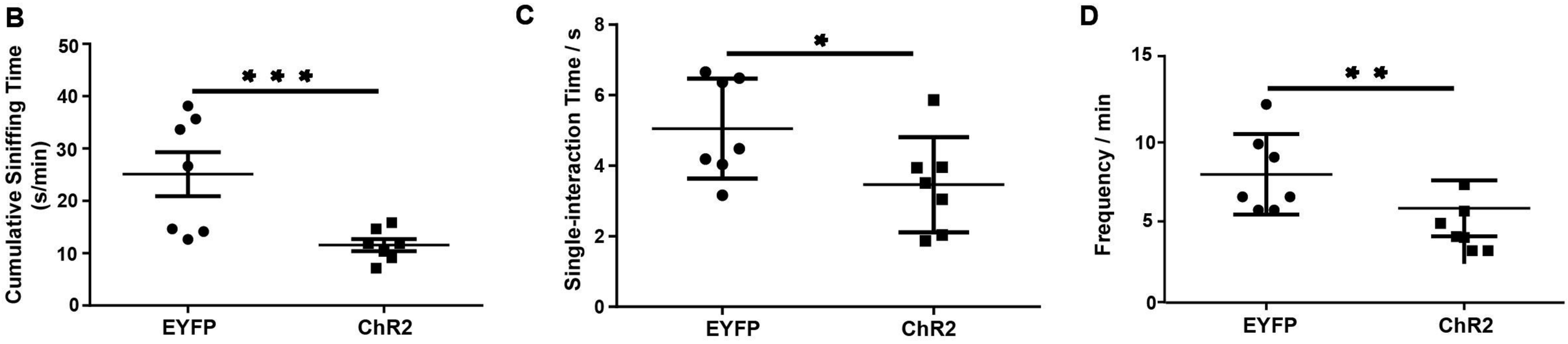

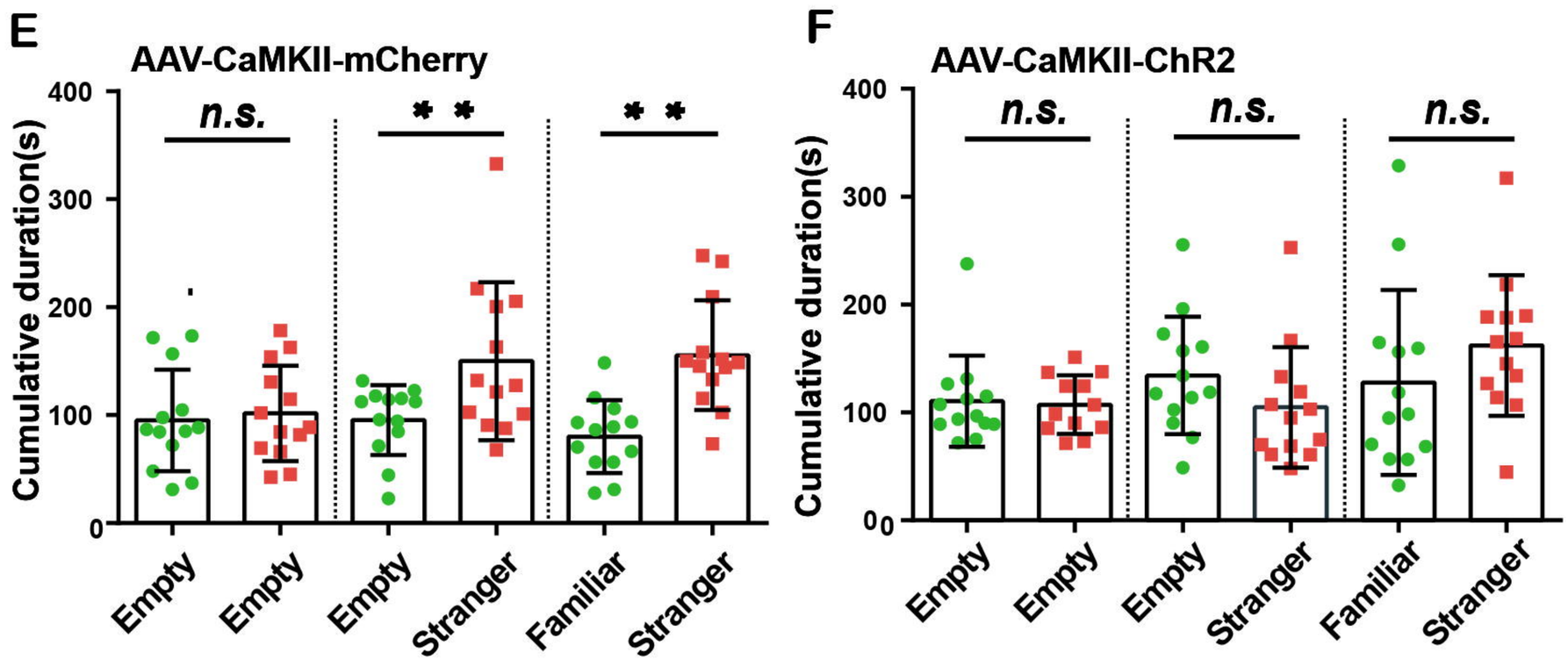

Continuous-inhibition with hSyn-GtACR

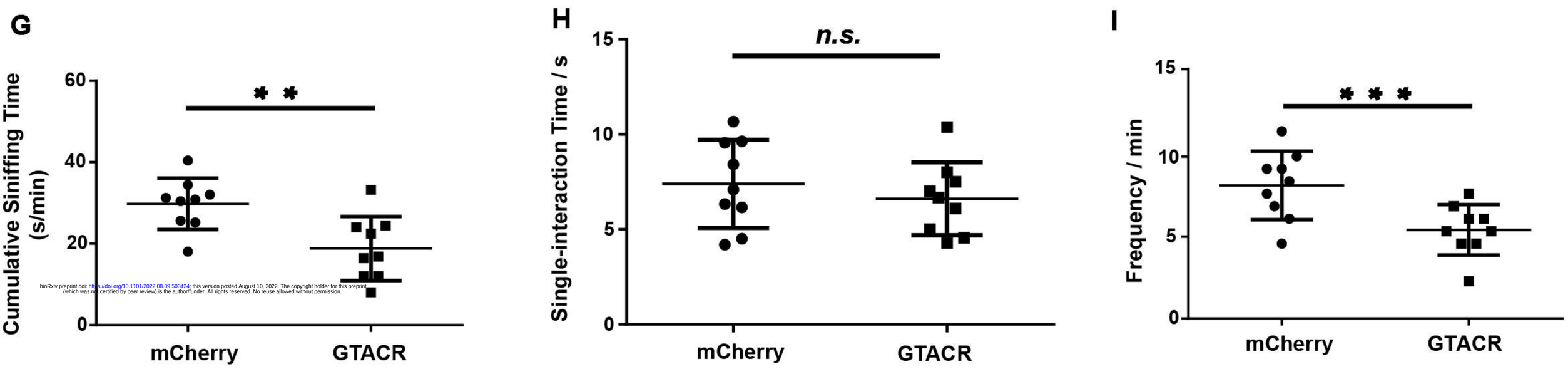

Sniffing start-inhibition with hSyn-GtACR

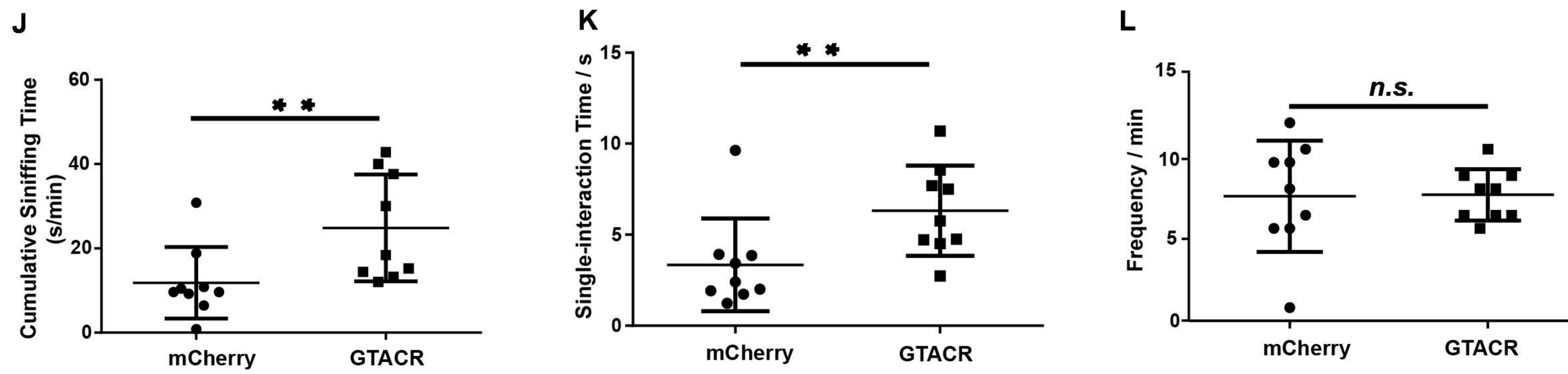

Shi et al. Figure 3

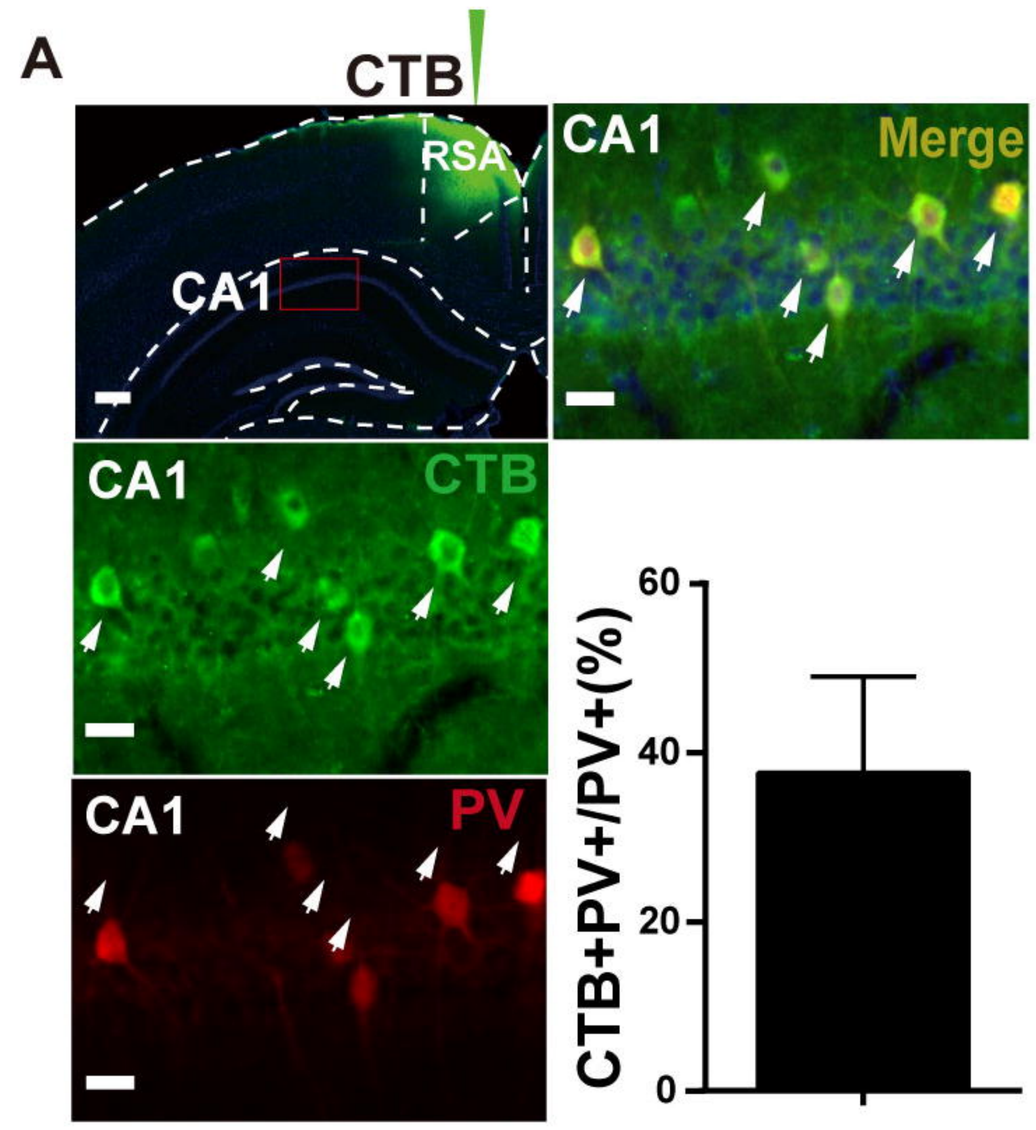

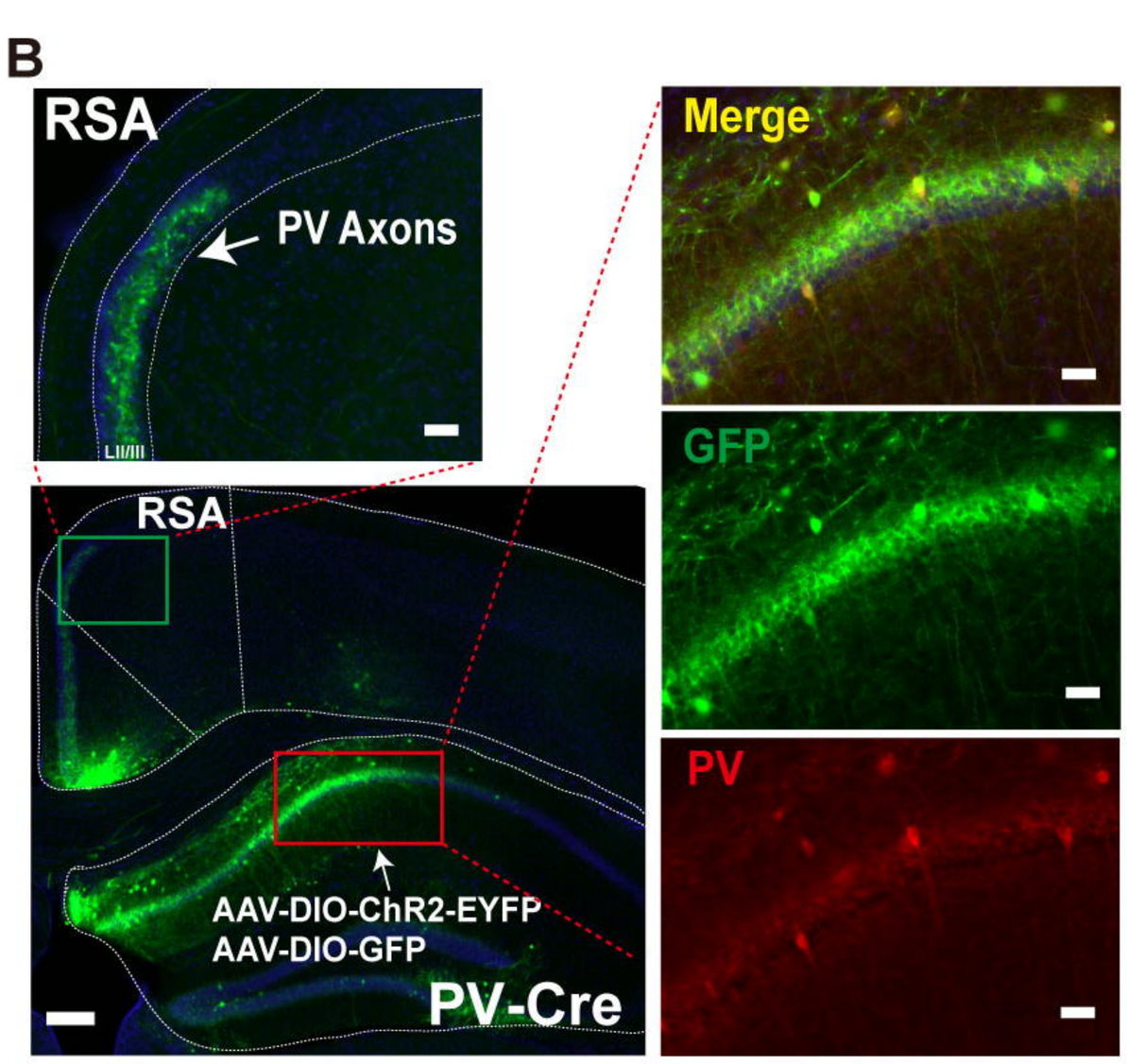

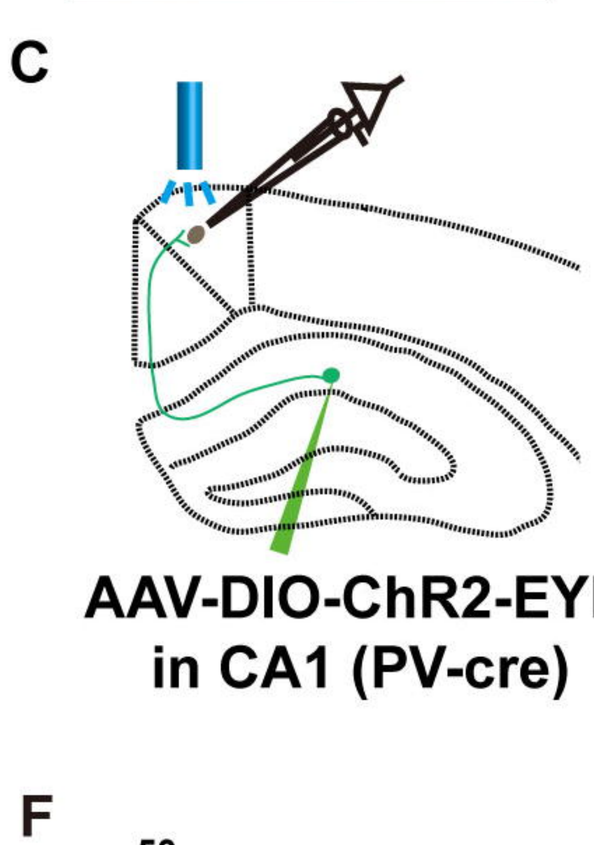

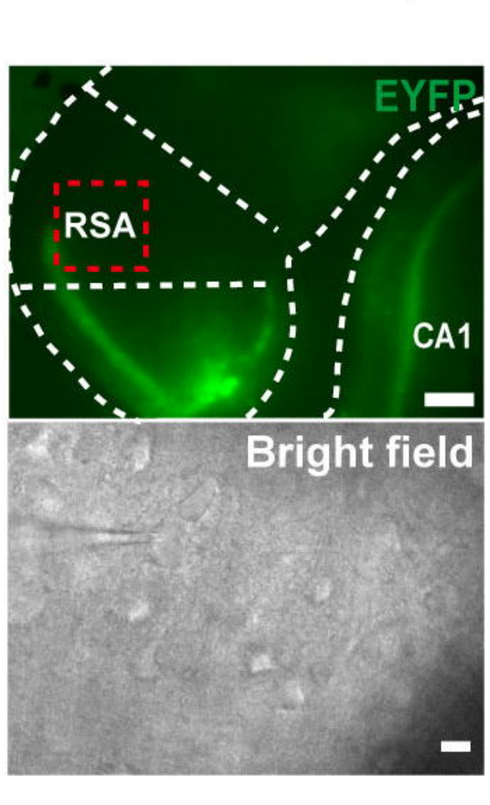

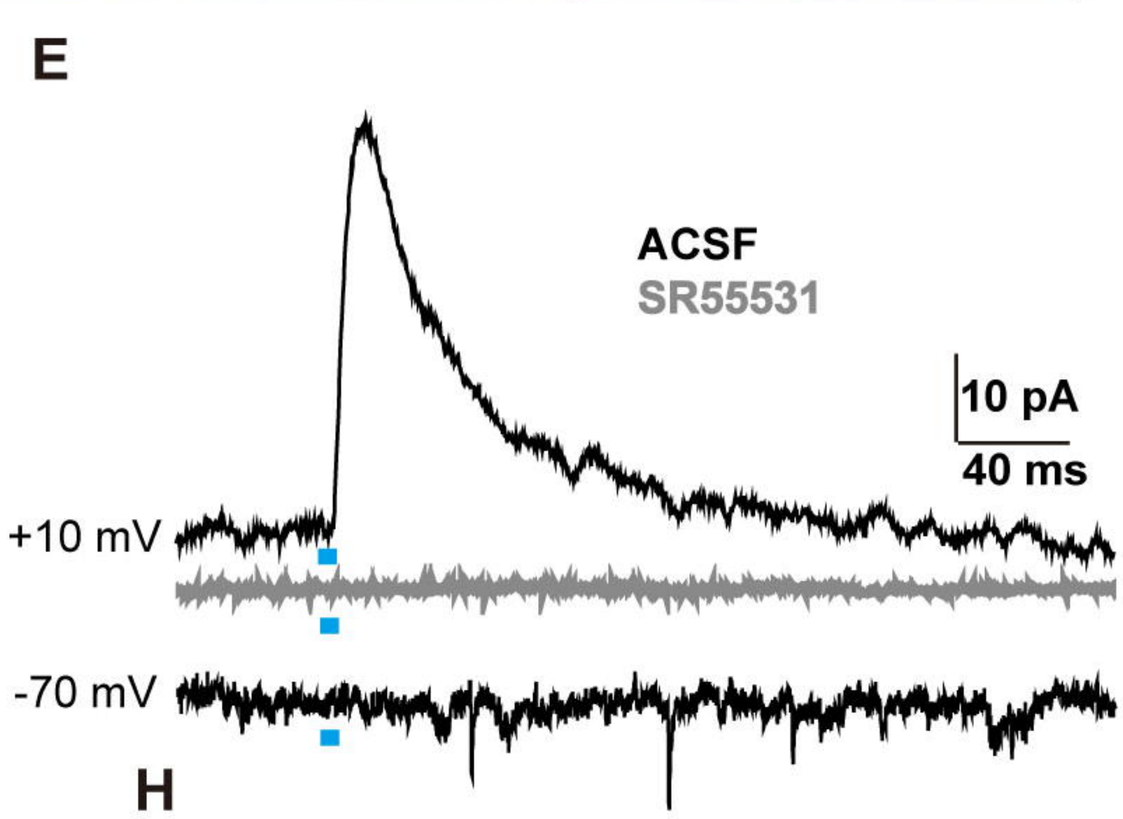

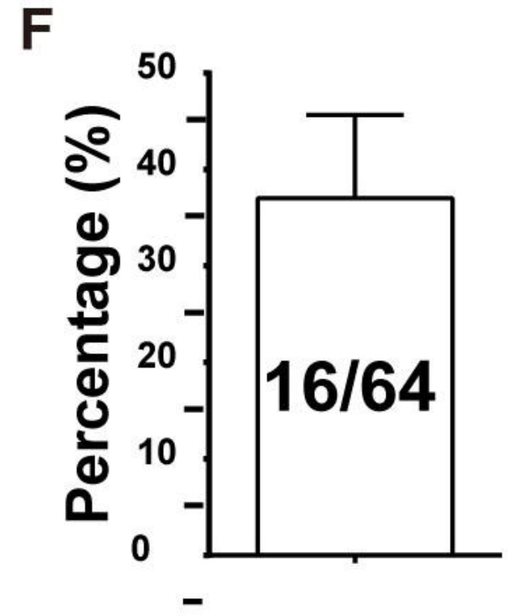

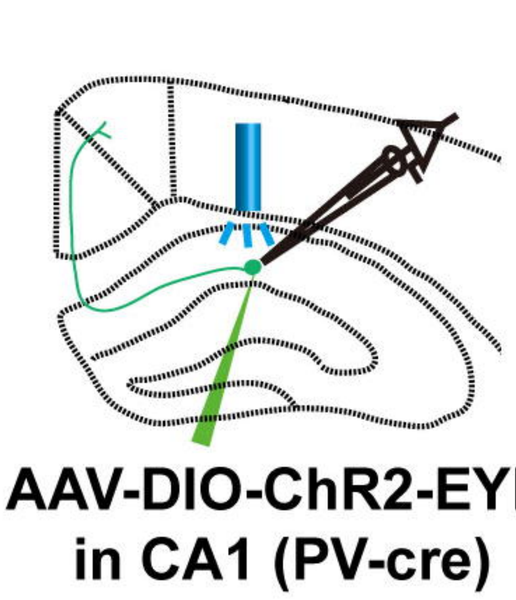

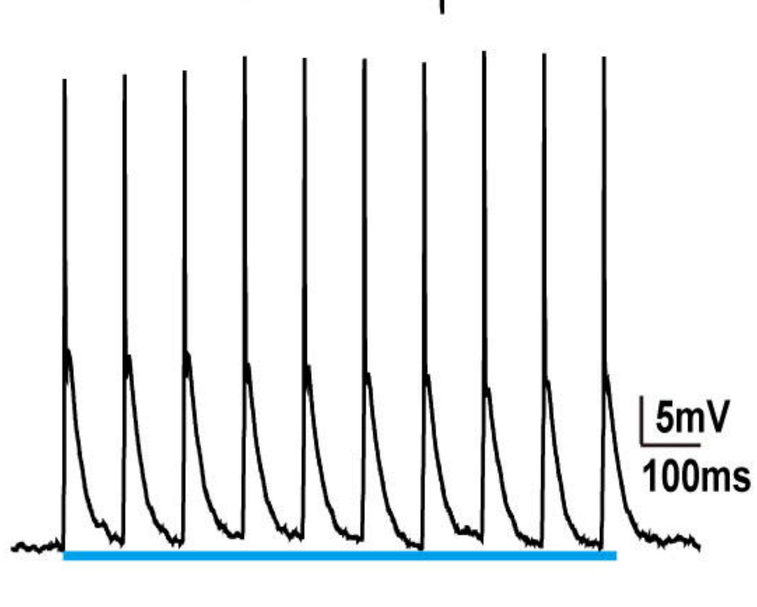

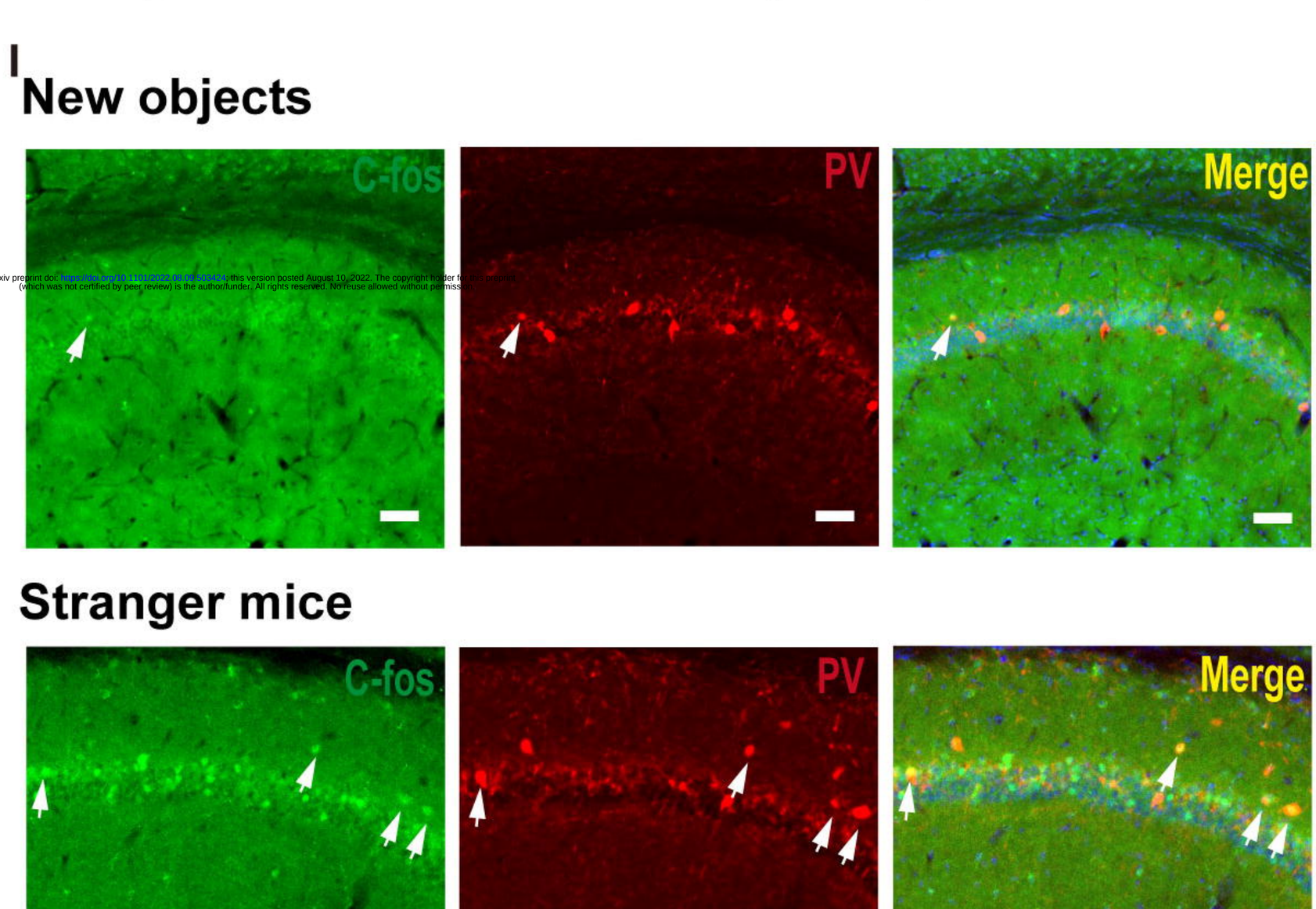

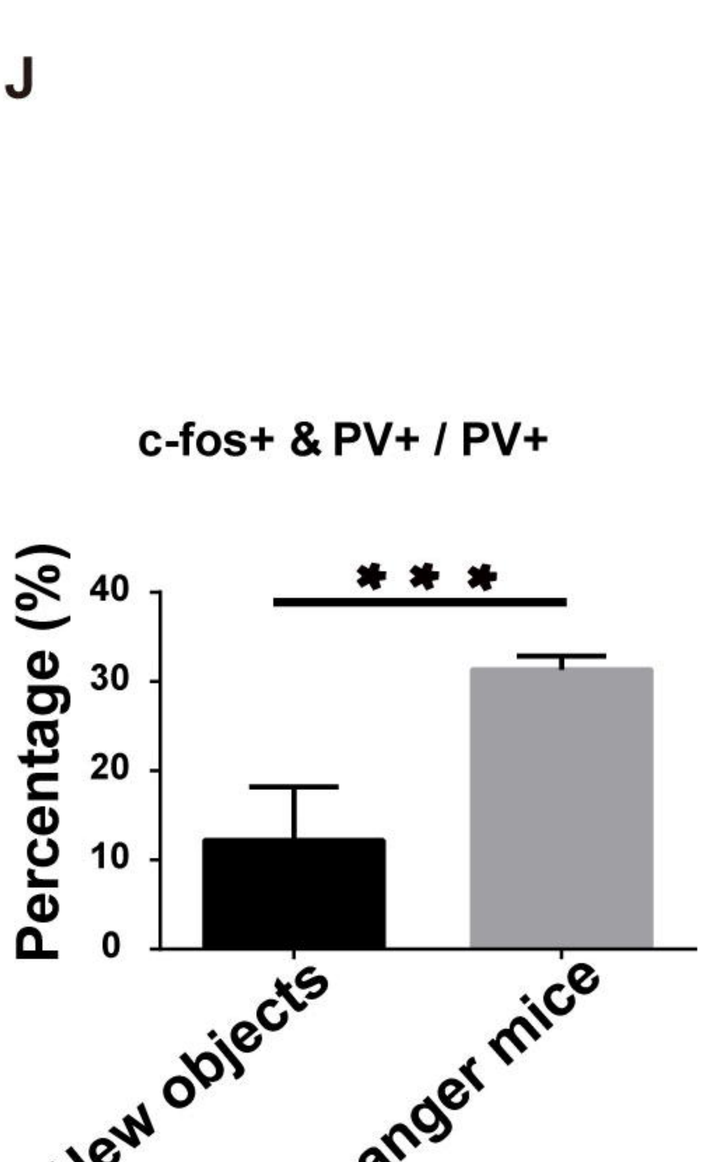

Shi et al. Figure 4

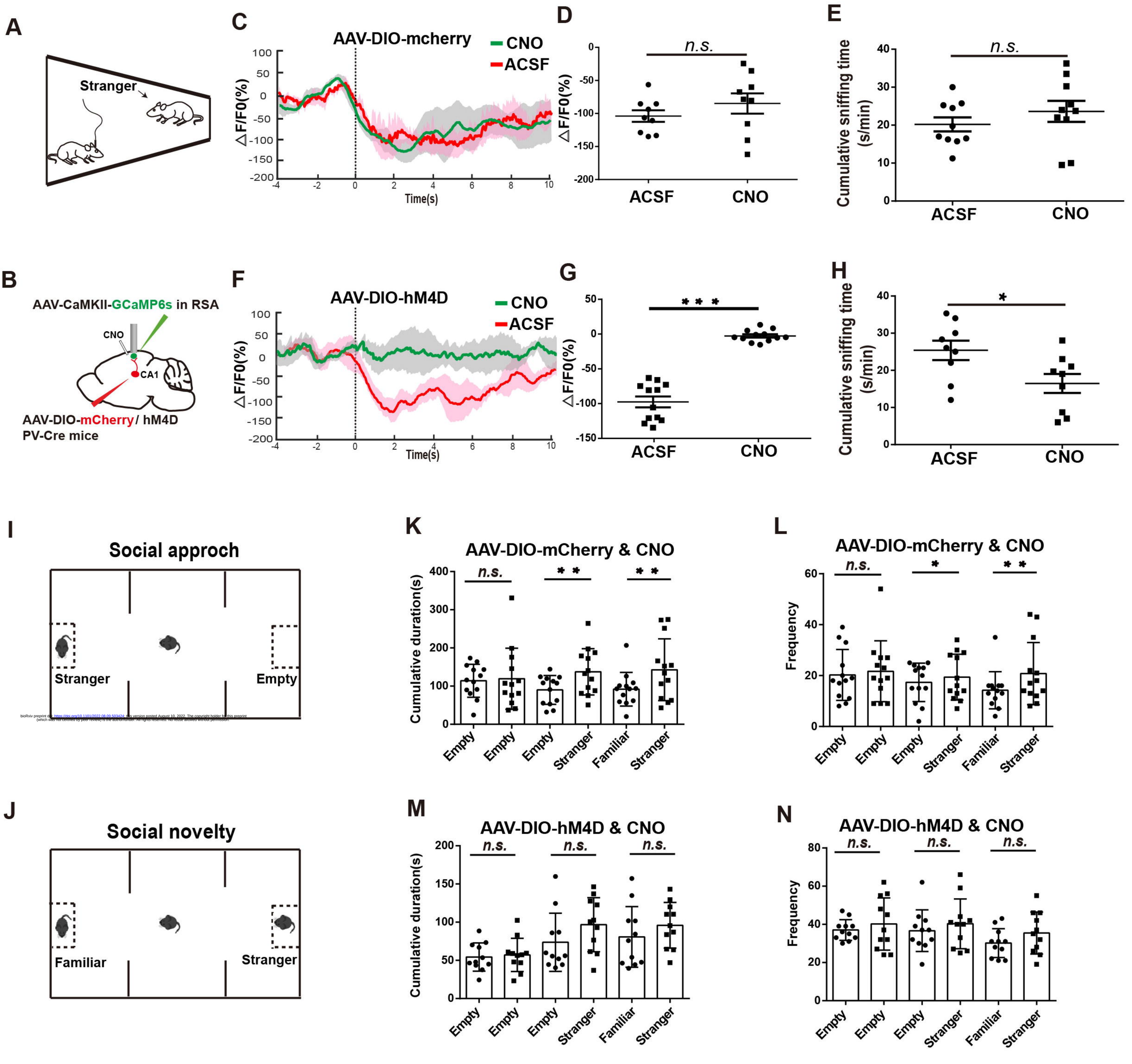

Shi et al. Figure 5